nature materials

Article

https://doi.org/10.1038/s41563-026-02555-0

# Amino acid-derived ionizable lipids enable inhaled base editing for therapeutic gene correction in the lung

Received: 19 May 2025

Accepted: 20 February 2026

Published online: 01 April 2026

Check for updates

Fanglin Gong[1,2,14], Yue Xu[1,14], Jingan Chen[1,2], Shun Zhang[3], Songtao Dong[1], Lauren Healy[4], Breanna Seto[4], Muye Zhou[1], Rick Xing Ze Lu[1], Gen Li[1,2], Tyler Thomson[1,2], Yinghua Tang[5,6], Ziyan Chen[7,8], Krista Antonio[8,9], Andrew Varley[10], David X. W. Chen[1], Craig A. Hodges[11,12], Amy P. Wong[8,9], Jim Hu[7,8], Basil P. Hubbard[3], John F. Engelhardt[5,6], Ziying Yan[5,6] & Bowen Li[1,2,4,13]

CRISPR-based gene editing holds promise for treating genetic diseases, yet its application to lung disorders has been hindered by the challenges of pulmonary delivery. Inspired by the modularity and biocompatibility of amino acid-derived chemistries, we report the combinatorial synthesis of 960 ionizable lipids incorporating chemically diverse backbones from both proteinogenic and non-proteinogenic α-amino acids. Through high-throughput screening and structure–function analysis, we identify CHCha-10, a cyclohexyl amino acid-derived lipid that forms biodegradable nanoparticles capable of efficiently delivering mRNA-based gene editors to lung epithelial cells. Following intratracheal administration, CHCha-10 nanoparticles exhibit enhanced mucus penetration and epithelial-specific transfection in both mice and ferrets. Here, as a functional application, we demonstrate in vivo base editing in the lung via inhalation. Delivery of adenine base editor mRNA and guide RNA targeting the *CFTR* G542X mutation restores CFTR expression and chloride channel function in G542X human airway epithelial cells, mouse-derived intestinal organoids and the lungs of cystic fibrosis mice. This work establishes a chemically modular design framework for ionizable lipids and a translatable platform for RNA-based pulmonary gene correction.

Clustered regularly interspaced short palindromic repeats (CRISPR)-based gene editing has emerged as a revolutionary technology for durable, precise and programmable correction of disease-causing genetic mutations. Although conventional CRISPR–Cas9 systems have shown promise in preclinical and clinical settings, their reliance on DNA double-strand breaks and endogenous repair pathways introduces risks such as indels, chromosomal rearrangements and unpredictable outcomes[1]. To overcome these limitations, base editors were developed as a next-generation CRISPR tool that enables precise single-nucleotide conversions without double-strand breaks[2]. Among these, adenine base editors (ABEs) enable targeted conversion of an adenine–thymine (A–T) base pair into a guanine–cytosine (G–C) base pair in the DNA sequence and are particularly suited for correcting pathogenic point mutations[3]. The therapeutic potential of base editing was recently underscored by the first reported use of a personalized CRISPR base editor in a human patient, in which a bespoke therapy corrected a lethal CPS1 mutation in a 10-month-old child[4].

A full list of affiliations appears at the end of the paper. e-mail: bw.li@utoronto.ca

Despite this milestone and continued advances in editor engineering, in vivo delivery remains a fundamental barrier to extending gene-editing therapies to extra-hepatic tissues, particularly the lung. Adeno-associated virus vectors have been widely used for gene editing, but their utility is constrained by key limitations. Their small packaging capacity often necessitates truncated editor variants[5,6] or dual-vector systems[7–12] for large constructs such as ABEs, complicating delivery. In addition, as DNA-based vectors, adeno-associated virus mediate prolonged expression of gene-editing machinery, increasing the risk of insertional mutagenesis and immune responses[13]. These safety concerns[14], coupled with the inability to administer repeat doses due to immunogenicity[15], greatly limit their translational potential.

Lipid nanoparticles (LNPs) have emerged as a clinically validated, non-viral alternative, offering transient expression, broad cargo compatibility and the potential for repeat dosing. Although LNPs enabled the success of mRNA vaccines and liver-targeted gene therapies[16–20], extending this platform to the lung presents unique challenges. Inhaled LNPs must penetrate airway mucus layers, evade mucociliary clearance and efficiently transfect target cells while maintaining structural integrity[21]. Achieving robust transfection in airway epithelial cells remains a critical hurdle to realizing the therapeutic potential of mRNA and gene-editing tools for pulmonary diseases such as cystic fibrosis (CF).

Among the four canonical components of LNPs, ionizable lipids, helper lipids, cholesterol and PEG lipids, the ionizable lipid plays a central role in determining delivery potency, biocompatibility and cell specificity[22–25]. However, efforts to expand the structural diversity of biodegradable ionizable lipids have been limited by synthetic bottlenecks and a lack of rapid and modular synthesis strategies. Ugi-based multi-component reactions have been used to swiftly generate combinatorial lipid libraries with diverse chemical properties[26]. However, traditional implementations of this approach typically require catalysts to achieve high yields and additional synthesis steps to introduce biodegradable bonds, which limit scalability and throughput[27].

Here, we address these challenges by developing a catalyst-free, amino acid-based Ugi five-centre-four-component reaction (Ugi-5C-4CR) to synthesize a chemically diverse ionizable lipid library with built-in biodegradability. Using this platform, we generated a combinatorial library of 960 ionizable lipids incorporating both proteinogenic and non-proteinogenic α-amino acids, with broad chemical diversity and design flexibility. These lipids were systematically screened for mRNA delivery efficiency in two dimensions and air–liquid interface (ALI) human bronchial epithelial (HBE) cell cultures. Through high-throughput screening and structure–function analysis, we identified CHCha-10, a cyclohexyl amino acid-derived lipid, as the lead candidate, exhibiting superior epithelial transfection efficiency and biocompatibility. When formulated into LNPs and administered intratracheally, CHCha-10 achieved efficient and widespread mRNA delivery to lung epithelial cells in both mice and ferrets. The resulting gene editing spanned major epithelial subtypes, including basal, club, ciliated cells, and ionocytes, and are critical targets in CF pathology, while minimizing off-target delivery to endothelial and immune cells. To assess therapeutic applicability, we employed CHCha-10 LNPs for the pulmonary delivery of mRNA encoding an ABE (mABE) and a single guide RNA (sgRNA) targeting the *CFTR* G542X nonsense mutation in a CF mouse model. Inhaled administration achieved over 12% on-target base editing in lung epithelial cells and led to a 60% increase in CFTR protein expression. Moreover, in both *CFTR* G542X HBE cells and intestinal organoids derived from *CFTR* G542X CF mice, CHCha-10 LNP-mediated base editing restored CFTR-dependent chloride channel activity, confirming functional correction of the disease-causing mutation. These findings establish CHCha-10 LNPs as a translatable non-viral platform for pulmonary gene editing. This work demonstrates *in vivo* base editing in the lung via inhalation, marking an important advance towards precision gene therapies for CF and other respiratory disorders.

## Efficient mRNA delivery to lung epithelial cells by CHCha-10 LNPs

Ionizable lipids have previously been synthesized via the classical Ugi four-component reaction (Ugi-4CR)[28,29] and a Lewis acid-catalysed Ugi three-component reaction (Ugi-3CR)[27,30] (Supplementary Fig. 1). Building on these approaches and inspired by the modularity and biocompatibility of amino acid-derived chemistries, we now introduce a one-pot, catalyst-free Ugi-5C-4CR to develop a diversified generation of ionizable lipid libraries. This reaction combines aliphatic aldehydes, α-amino acids, isocyanides and methanol to generate α-acylamino-α-amino acid methyl ester derivatives bearing ionizable moieties (Fig. 1a). Compared with prior strategies, this platform offers expanded chemical diversity, improved modularity and biocompatibility through the incorporation of diverse and biocompatible amino acid building blocks owing to two ester bonds and two amide bonds within the molecular scaffold (Fig. 1a). Using a robotic liquid handler, we synthesized a combinatorial library of 960 structurally unique ionizable lipids in a single day[30] (Fig. 1b and Supplementary Fig. 2a). These lipids were formulated into LNPs using classical molar ratios[30] with 1,2-dioleoyl-*sn*-glycerol-3-phosphoethanolamine (DOPE), C14-$PEG_{2000}$ and cholesterol, which were loaded with firefly luciferase mRNA (mFluc). Transfection efficiency was evaluated in BEAS-2B cells derived from normal human bronchial epithelium by quantifying luminescence 24 h post treatment and normalizing to untreated controls (Supplementary Fig. 2b). The inclusion of diverse α-amino acid backbones substantially increased the chemical diversity of the ionizable lipid pool, improving mRNA delivery efficiency while maintaining favourable biocompatibility[19] (Fig. 1c). Structural analysis across the 960-member LNP library identified cyclohexylglycine derivatives as the most potent candidates when ranked by amino acid substructure (Fig. 1d). To elucidate how individual lipid components contribute to transfection performance, the structural features of the top 20 ionizable lipids were systematically examined (Fig. 1e). Notably, 80% of the top-performing candidates featured cyclic headgroups, suggesting a strong correlation between ring rigidity and delivery efficiency. Amino acid-derived ionizable lipids with rigid cyclic headgroups adopt more stable three-dimensional conformations than those with linear headgroups (LH), potentially enhancing mRNA complex stability through strengthened π-stacking[31]. This finding aligns with previous studies of high-performing ionizable lipids, such as cKK-E12[32], C12-C200[33] and OF-Deg-Lin[34], where the rigidity of the cyclic core was associated with enhanced delivery efficiency. Furthermore, the top LNPs displayed substantial amino acid diversification, with 13 structurally distinct amino acid derivatives represented among the most active candidates. This underscores the utility of amino acid-based combinatorial design in expanding the accessible chemical space of ionizable lipids. Further analysis revealed that 65% of the top performers incorporated highly branched hydrophobic tails (tail 10 and 11), indicating that branched tail structure is another key determinant of transfection efficiency, probably by modulating lipid packing and membrane-disruption properties.

## Enhanced epithelial mRNA delivery by optimized CHCha-10 LNPs

To mimic the relatively impermeable mucus barrier of lungs, an ALI culture model with an artificial mucus layer was employed[35]. The top 20 LNP candidates identified in the initial screen were tested in this model (Fig. 2a, Supplementary Fig. 3 and Supplementary Note 1). Consistent with the findings from the top 20 candidates identified in the non-differentiated cell screening, CHCha-10 LNPs synthesized using β-cyclohexyl-alanine (a non-proteinogenic amino acid with a cyclohexyl group on the β-carbon), demonstrated superior transfection potency across both non-differentiated and differentiated cell models (Fig. 2a and Supplementary Figs. 4 and 5). We also found the zeta potential of CHCha-10 LNPs was −0.126 mV (Supplementary Fig. 6), which falls within the range (0 to −5) reported to be favourable for penetrating

https://doi.org/10.1038/s41563-026-02555-0

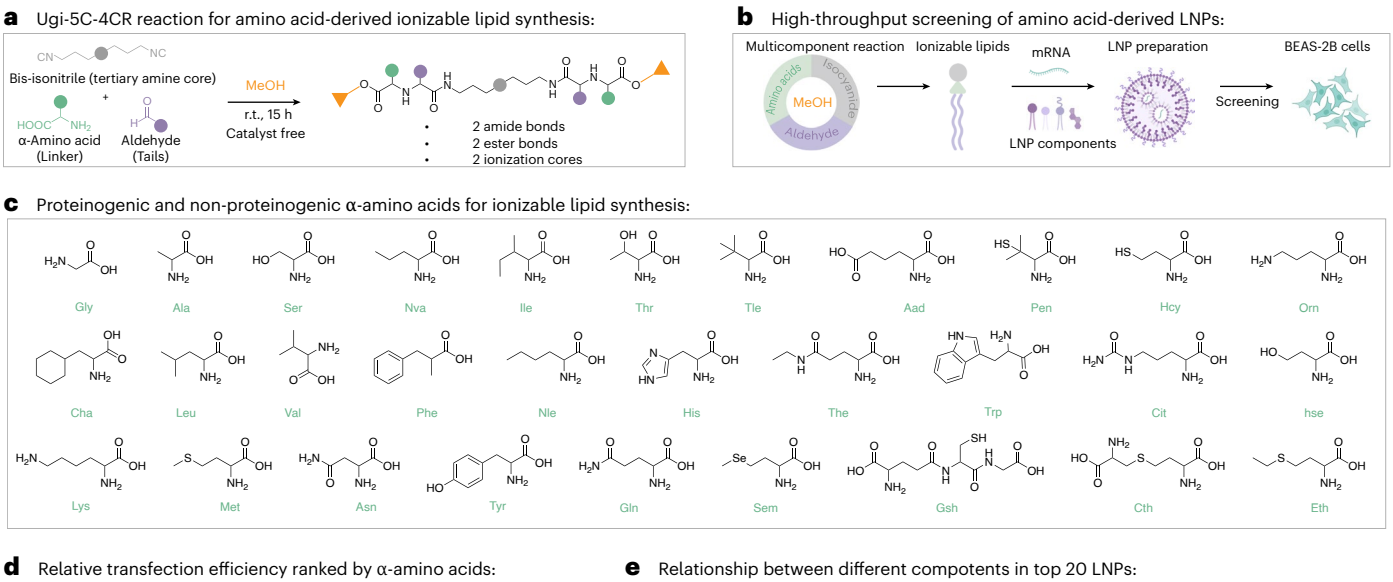


**Fig. 1 | Amino acid-derived ionizable LNPs for targeting lung epithelial cells.** **a**, Ugi-5C-4CR for amino acid-derived ionizable lipid construction, along with the corresponding Markush structure representing this reaction class. **b**, A workflow depicting the synthesis of amino acid-derived lipids, subsequent LNP formulation and their in vitro screening and validation process. **c**, A chemically diverse panel of proteinogenic and non-proteinogenic α-amino acids is employed for the synthesis of ionizable lipids in the Ugi-5C-4CR library. **d**, BEAS-2B cells were treated with mFluc-encapsulated LNPs. The relative luciferase expression was measured, normalized to untreated groups and presented as a $\log_2$ value. For each of the thirty amino acid-derived LNP formulations, the relative transfection efficiency was calculated by normalizing its normalized relative luciferase signal to that of the highest-performing amino acid-derived formulations. The normalized efficiencies were rank-ordered and visualized as a polar diagram. **e**, The relationship between different components in the top 20 LNPs, illustrated by a Sankey diagram. r.t., room temperature. Schematic in **b** created in BioRender; Li, B. https://biorender.com/v5gq5y2 (2026).

acidic mucus, compared with either strongly positive or strongly negative surface charges observed in other formulations[36,37]. To investigate the improved performance of CHCha-10 LNPs compared with cKK-E12, we used fluorescence resonance energy transfer (FRET) experiments to assess their endosomal fusion ability[26] (Fig. 2b). Compared with cKK-E12 LNPs, CHCha-10 LNPs exhibited stronger and faster membrane fusion and disruption (Fig. 2b). Furthermore, a fluorogenic probe, 6-(*p*-toluidino)-2-naphthalenesulfonic acid sodium salt (TNS), was used to evaluate the apparent pKa of LNPs (Fig. 2c). The apparent pKa of CHCha-10 LNPs (7.038) was similar to that of cKK-E12 (6.972), supporting their efficient endosomal escape capability (Fig. 2c). The enhanced performance of CHCha-10 might be attributed to the unique features of its cyclohexyl side chain, which facilitates hydrophobic interactions. These interactions enable the lipid to adopt a cone-shaped configuration, promoting the formation of non-bilayer structures, such as the hexagonal H-II phase.

We further utilized a design of experiments (DoE) approach[38] to improve the performance of CHCha-10 LNPs for mFluc delivery in BEAS-2B cells. Two rounds of DoE were conducted with various parameters: ionizable lipid-to-mRNA ratio, ionizable lipid composition, phospholipid composition, phospholipid types, cholesterol types and PEGylated lipid composition (Fig. 2d,f). The first round was to identify a suitable helper lipid for lung delivery (Fig. 2d). We chose DOPE, 1,2-dipalmitoyl-*sn*-glycero-3-phosphocholine (DPPC), 1,2-distearoyl-*sn*-glycero-3-phosphocholine (DSPC) and (2,3-dioleoyloxy-propyl)-trimethylammonium-chloride (DOTAP) as four types of helper lipid and generated formulations 1–24 (H1–H24; Fig. 2e and Supplementary Table 1) given that the cationic lipid DOTAP may improve pulmonary cell internalization and mucus retention[39,40]. DPPC and DSPC may promote mRNA release from endosomes due to their phase transition in endosomes[41]. DOTAP was identified as the top-performing helper lipid for the second round for mFluc (Fig. 2e). β-sitosterol, stigmasterol and cholesterol were chosen for the second round given that β-sitosterol and stigmasterol help endosomal fusion and intracellular retention of LNPs[42], leading to further increased transfection efficacy (Fig. 2f). Formulations C1–C18 were generated with these sterols (Fig. 2f and Supplementary Table 2). Formulation C1 exhibited superior delivery of mFluc in BEAS-2B cells (Fig. 2g) and ALI-cultured BEAS-2B cells with artificial sputum medium (Supplementary Fig. 7). This optimized formulation was then evaluated for pulmonary delivery of mFluc, showing a sixfold improvement over cKK-E12 LNPs (Fig. 2h,i).

https://doi.org/10.1038/s41563-026-02555-0

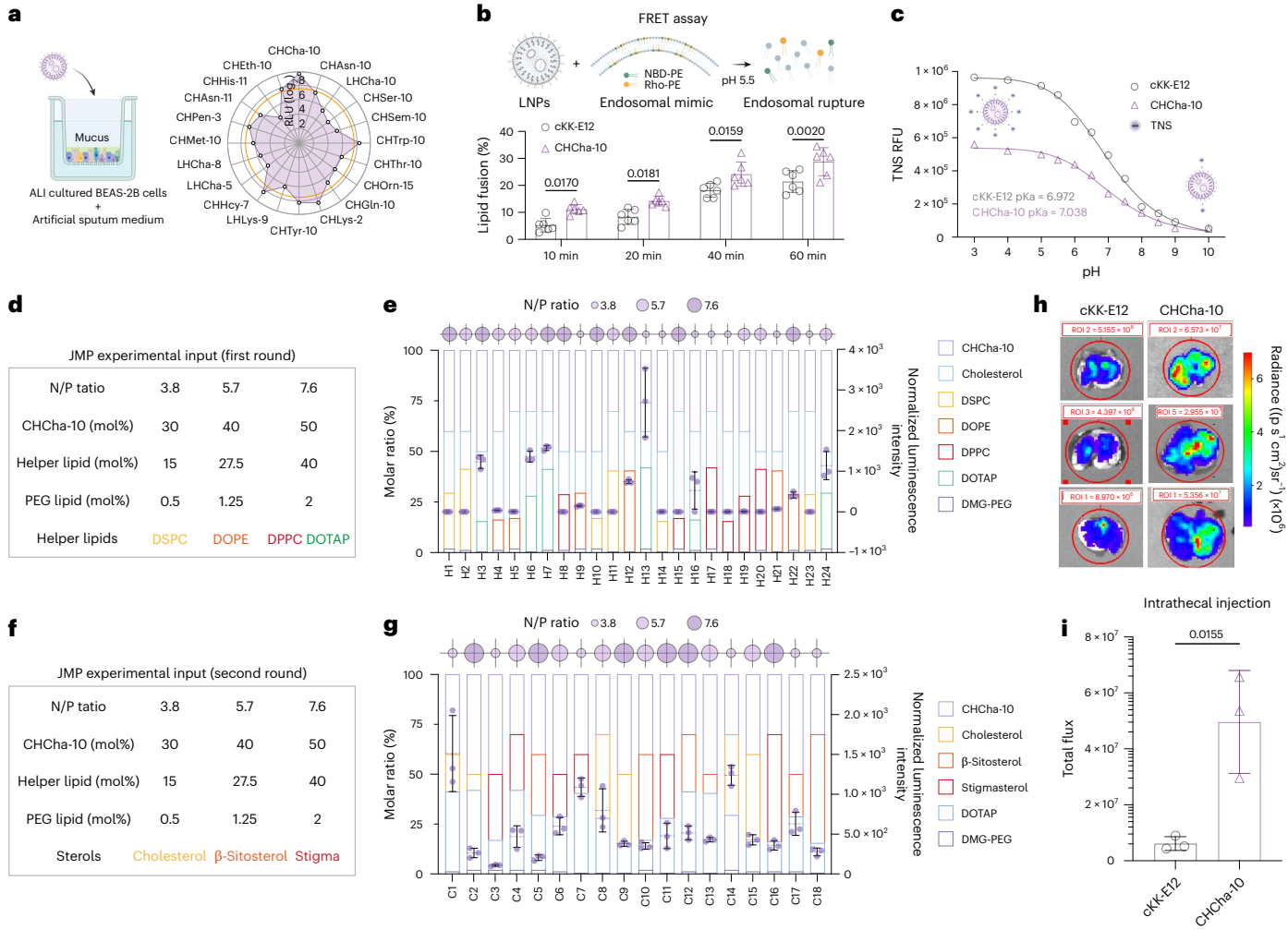


**Fig. 2 | Characterization and formulation optimization of the CHCha-10 lipid.** **a**, A screening of the top 20 lipids in differentiated BEAS-2B cells compared with cKK-E12. The radar diagram showed the normalized relative luciferase expression ($log_2$ value) in treated differentiated BEAS-2B cells ($n = 3$). The normalized relative luciferase expression of cKK-E12 was indicated by the yellow line. **b**, A schematic and quantitative results of endosomal rupture by LNPs at different time intervals ($n = 6$, ordinary two-way analysis of variance). **c**, Representative TNS titration curves for LNP-apparent pKa ($n = 3$). Sigmoidal best-fit analyses in GraphPad Prism 10 were used to determine pKa as the pH at half-maximum relative fluorescent units (RFU). **d**, JMP input parameters for the first round of DoE. **e**, Molar ratios and the relative luciferase expression of the 24 LNP formulations in the first round of DoE ($n = 3$). **f**, JMP input parameters for the second round of DoE. **g**, Molar ratios and the relative luciferase expression of the 18 LNP formulations in the second round of DoE ($n = 3$). **h**, IVIS images of mouse lungs 6 h after intratracheal administration of mFluc-loaded cKK-E12 or CHCha-10 LNPs (0.3 mg $kg^{-1}$ total RNA). **i**, Quantification results of luminescence intensity from IVIS images ($n = 3$, two-tailed unpaired Student's *t*-tests). The data are presented as mean values ± s.d. in **b**, **e**, **g** and **i**. Schematics created in BioRender: **a**, Li, B. https://biorender.com/d1vmi2w (2026); **b**, Li, B. https://biorender.com/s420olp (2026); **c**, Li, B. https://biorender.com/axwsdv6 (2026).

## CHCha-10 LNPs deliver mCre to mouse and ferret epithelium

Building on the strong mFluc delivery efficacy of CHCha-10 LNPs in mouse lungs, we next assessed their potential for gene editing in lung cell populations. Intratracheal administration of CHCha-10 LNPs encapsulating Cre mRNA (mCre) was conducted in Ai9 reporter mice at 0.75 mg/kg per dose (three doses, 12.8:1 total lipid:RNA ratio) (Fig. 3a). In these mice, Cre-mediated recombination at loxP-flanked '3x STOP' sites can activate tdTomato expression (Fig. 3a, Supplementary Fig. 8). CHCha-10 LNPs achieved 28.8% editing in lung epithelial cells, nearly doubling the 14% efficiency of cKK-E12 LNPs (Fig. 3b,c and Supplementary Fig. 9), while maintaining low editing efficiencies in immune cells (1.72%) and endothelial cells (0.53%). The stronger tdTomato signal observed in epithelial cells probably results from the intratracheal administration route, which directly delivers LNPs to the airway epithelium, consistent with previous findings[43]. For CHCha-10, this epithelial preference is more pronounced than for cKK-E12 under identical delivery conditions (Fig. 3c), probably because CHCha-10 was screened using lung epithelial cells and thus shows higher tropism towards this cell population compared with the benchmark. To investigate phenotypes of edited cells, we evaluated club (secretory) cells, ciliated cells, basal cells, and ionocytes, each of which plays a critical role in airway epithelial homeostasis and are directly impacted by loss of CFTR function[44,45]. Basal cells represent the main stem/progenitor compartment of the airway epithelium, endowed with long-term self-renewal capacity and the ability to differentiate into all major luminal cell types[21,46]. Because of this durable regenerative potential, targeting basal cells is essential for gene-editing therapies: edits introduced here can persist and propagate through successive waves of airway epithelial renewal, thereby enabling durable correction rather than transient effect. Meanwhile, onocytes, which express the highest levels of CFTR in the airway epithelium, represent another important target population for CF gene editing[21,47]. However, unlike human lungs, the distal airways of mice contain minimal basal cells or ionocytes[48]. To account for this species-specific

https://doi.org/10.1038/s41563-026-02555-0

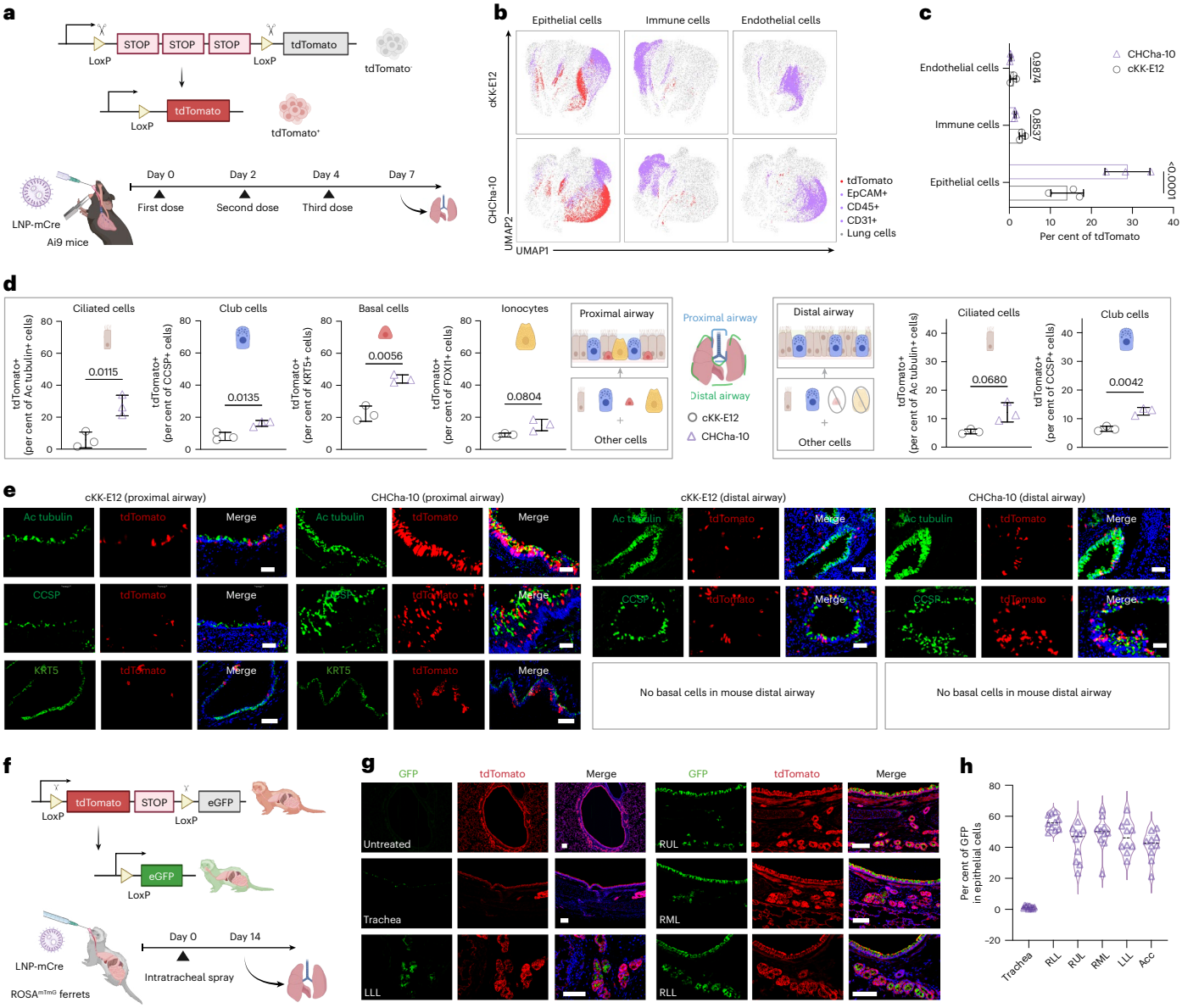


**Fig. 3 | CHCha-10 LNPs for mCre delivery to mouse and ferret epithelium.** **a**, A schematic of the experimental procedure for assessing editing efficiency of CHCha-10 LNPs loaded with mCre in Ai9 reporter mice. Mice treated with cKK-E12 LNPs served as controls. **b**, A uniform manifold approximation and projection display showing the proportion of tdTomato-positive epithelial, endothelial and immune cells among lung cells. **c**, Flow cytometry quantifying the percentage of the tdTomato-positive of epithelial, endothelial and immune cells among lung cells ($n = 3$, ordinary two-way analysis of variance, 0.0000954301). **d**, The proximal airway data show the percentage of tdTomato-positive ciliated, club, basal and ionocyte cells. Distal airway data show the percentage of tdTomato-positive ciliated and club cells ($n = 3$, unpaired $t$-test with Welch's correction). **e**, Representative immunofluorescence images of lung sections from LNP-treated Ai9 reporter mice, illustrating LNP-mediated gene editing in distinct lung epithelial cell populations ($n = 3$, merging of tdTomato (red) with DAPI (blue) produced a purple signal; scale bar, 50 µm). **f**, A schematic of mCre LNP-mediated gene editing in juvenile ferret lungs. **g**, Representative confocal images of different lung lobes in ferrets treated with CHCha-10 LNPs, stained with anti-GFP and anti-tdTomato antibodies. Images from the RUL, RML, RLL and LLL highlight transfected submucosal glands. Scale bar, 50 µm. **h**, A quantitative analysis of GFP-positive cell colocalization within manually selected epithelial cells across different lung lobes ($n = 10$ images per region, $n = 2$ biologically independent samples). The data are presented as mean values ± s.d. in **c** and **d**. The data are presented as mean with horizontal jitter reflecting data density at each $y$ value in **h**. Schematics created in BioRender: **a**, Li, B. https://biorender.com/oezefjt (2026); **d**, Li, B. https://biorender.com/jy58n29 (2026); **f**, Li, B. https://biorender.com/6wir6li (2026).

limitation, we analysed mouse proximal (trachea and primary bronchi) and distal (conducting and respiratory airways) segments separately, and excluded basal-cell and ionocyte assessments in the distal airway regions. In the proximal airways, CHCha-10 LNPs transfected 16.2% of club cells, 27.3% of ciliated cells, 44.0% of basal cells, and 15.2% of ionocytes (Fig. 3d, Supplementary Fig. 10). In the distal airways, editing efficiency was 12.6% for club cells and 12.2% for ciliated cells (Fig. 3d, Supplementary Fig. 10). CHCha-10 LNPs demonstrated superior editing efficiency compared to cKK-E12 LNPs across multiple epithelial subtypes. In the proximal airways, CHCha-10 LNPs achieved a 2-fold higher editing rate in basal cells and a 5.6-fold higher editing rate in ciliated cells compared to cKK-E12 (Fig. 3d). In the distal airways, CHCha-10 LNPs showed a 2.7-fold improvement in club cell editing (Fig. 3d). Immunofluorescence analysis further confirmed strong tdTomato signal colocalization in ciliated cells (Ac-tubulin-positive), basal cells (KRT5-positive), and club cells (CCSP-positive) in CHCha-10-treated lungs, whereas cKK-E12-treated lungs exhibited weaker colocalization (Fig. 3e). Notably, FACS results for basal, ciliated, and club cells showed

slightly higher background signals than confocal images, probably due to the cell permeabilization required for antibody staining (anti-KRT5, Ac-tubulin, and CCSP). Furthermore, mice treated with CHCha-10 LNPs showed cytokine levels comparable to PBS controls in both bronchoalveolar lavage fluid (BALF) and serum, whereas cKK-E12 LNPs resulted in marked elevations of GM-CSF levels in BALF and TNFα levels in serum (Supplementary Figs. 11 and 12), indicating improved biocompatibility of CHCha-10 LNPs compared with cKK-E12 LNPs.

The ferret CF disease model is widely recognized as a robust pulmonary disease model as it recapitulates key human lung disease phenotypes[49,50]. Due to the physiological similarities between ferrets and human lungs, mCre encapsulated in CHCha-10 LNPs was evaluated in ROSA$^{mTmG}$ transgenic ferrets to verify their potential translational ability. These ferrets carry a Cre-responsive reporter cassette (CAG-LoxP-tdTomato-Stop-LoxP-eGFP) integrated into the ROSA locus, enabling precise visualization of Cre-mediated recombination[23,51,52]. The cassette expresses membrane-bound tdTomato under basal conditions. Upon Cre recombinase expression, the tdTomato-STOP sequence is excised, activating membrane-bound enhanced green fluorescent protein (eGFP) expression and producing a red-to-green fluorescence switch in edited cells. Herein, we evaluated the performance of CHCha-10 LNPs in both ALI-differentiated primary basal cells derived from ROSA$^{mT/mG}$ ferrets and in the lungs of ROSA$^{mT/mG}$ ferrets directly via intratracheal administration (Fig. 3f and Supplementary Fig. 13). In ALI-differentiated primary ferret airway basal cells, CHCha-10 LNPs enhanced the colocalization of GFP-positive cells with markers for distinct epithelial subtypes, including club cells, ciliated cells and basal cells, compared with cKK-E12 LNPs (Supplementary Fig. 13). To further evaluate in vivo editing efficiency of CHCha-10 LNPs across different species, juvenile ferrets received a single dose of mCre encapsulated in CHCha-10 LNPs (0.6 mg kg$^{-1}$ mCre, 12.8:1 total lipid:total RNA ratio) (Fig. 3f). Two weeks post administration, lung tissues were collected and analysed for GFP-positive cells in the bronchus. Confocal imaging revealed robust editing in epithelial cells from the right lower lobe (RLL), right upper lobe (RUL), right middle lobe (RML) and left lower lobe (LLL), with moderate efficiency observed in the trachea (Fig. 3g,h). Moreover, images from the RLL, RML, RUL and LLL further highlighted efficient editing in submucosal glands, which are critical sites for CFTR protein production and are implicated in CF pathophysiology[53] (Fig. 3g). Furthermore, histological analysis via H&E staining demonstrated no evidence of inflammation in any lung lobes of ferrets dosed with CHCha-10 LNPs, supporting its biosafety profile (Supplementary Fig. 14). Compared with the recently reported FO-32 and FO-35 LNPs for pulmonary mRNA delivery in ferrets, CHCha-10 LNPs exhibited preferential transfection of the airway epithelium, with minimal editing in the alveolar regions, which are rich in immune and endothelial cells[23]. This localized delivery approach reduces off-target editing in non-epithelial lung cells, which is advantageous for minimizing potential adverse effects such as chromosomal translocations[54].

## Optimized ABE system corrects *CFTR* G542X

To evaluate the potential of CHCha-10 LNPs for delivering base editors in gene-editing therapy, we optimized the ABE system to correct the *CFTR* G542X mutation in both mouse and human genes. Due to the lack of a canonical PAM site within the editing window (A3–A9) for the G542X mutation in both mouse and human *CFTR*, we utilized the SpCas9 variant SpRY, which features an expanded PAM recognition profile[55]. To facilitate the process of identifying an optimal ABE system, we developed two reporter systems using the piggyBac (PB) transposon/transposase: one incorporating a premature stop codon (PTC) in Nanoluc luciferase (PTC_Nluc)[56] and another inserting a Fluc sequence upstream of mouse *Cftr*, centred on the G542X mutation (*Cftr* G542X_Fluc)[57] (Supplementary Note 2). These were stably integrated into the BEAS-2B human bronchial epithelium cell line, where successful T-to-C editing restores Nluc or Fluc expression, quantitatively reporting ABE on-target efficiency (Fig. 4a,d). To identify the optimal ABEs for efficient on-target editing, we tested four highly active ABEs in their SpRY forms, including ABE$_{max}$-SpRY[39], ABE$_{8.20}$-SpRY[58], ABE$_{8e}$-SpRY[58] and CE-ABE$_{8e}$-SpRY[59] alongside five sgRNAs designed to position the target adenine at A3–A8 relative to the PAM (Fig. 4b). All ABEs demonstrated on-target editing, as indicated by normalized Nluc luminescence intensity in treated PTC_Nluc BEAS-2B cells (Fig. 4c). PTC_Nluc BEAS-2B cells treated with these ABEs also exhibited increased Nluc mRNA levels, as quantified by the reverse transcription–quantitative polymerase chain reaction (RT–qPCR), which were consistent with the corresponding increases in Nluc luminescence intensity (Fig. 4c and Supplementary Fig. 15). Among these, ABE$_{8e}$-SpRY and CE-ABE$_{8e}$-SpRY exhibited higher editing efficiency compared with ABE$_{max}$-SpRY and ABE$_{8.20}$-SpRY (Fig. 4c), aligning with previous findings[58–60]. Based on the activity of ABEs and the strategy of positioning target adenines at later positions (A6–A13) within the actual CFTR target site to minimize bystander editing, we selected ABE$_{8e}$-SpRY and CE-ABE$_{8e}$-SpRY for further studies. Meanwhile, CE-ABE$_{8e}$-SpRY mRNA and chemically modified Nluc-A8 sgRNA were used to optimize the mRNA-to-sgRNA ratio in PTC_Nluc BEAS-2B cells. The results showed no statistical differences in editing efficiency across the tested ratios (Supplementary Fig. 16). Based on these results and previous studies[16,17], a 1:1 weight ratio was selected for all subsequent studies.

To optimize editing specificity and minimize bystander edits, we tested six sgRNAs with different PAMs against the *CFTR* G542X gene in combination with the two optimal ABEs in the *CFTR* G542X_Fluc BEAS-2B cell line (Fig. 4d,e). CE-ABE$_{8e}$-SpRY exhibited higher activity at positions A7-A9, whereas ABE$_{8e}$-SpRY was more active at A4-A6 by both the luminescence intensity of the Fluc protein and the relative Fluc mRNA levels (Fig. 4f and Supplementary Fig. 17). Notably, the combination of CE-ABE$_{8e}$-SpRY mRNA and an sgRNA targeting A9 (PAM = NYN) achieved the maximal luminescence signal and the highest Fluc mRNA level (Fig. 4f and Supplementary Fig. 17). Sanger sequencing showed that CE-ABE$_{8e}$-SpRY and sgRNA A9 achieved ~60% T-to-C conversion with near-background levels of bystander editing (Fig. 4g). Based on these results, CE-ABE8e-SpRY mRNA was selected for all subsequent experiments and is hereafter referred to as mABE.

## CHCha-10 LNP achieve CFTR restoration in CF mouse lungs

The size of the RNA molecule has been previously shown to affect LNP delivery efficiency[61]. Given that base editors are substantially larger than Fluc and Cre recombinase, we re-optimized the CHCha-10 LNP formulation using a reporter mRNA encoding ABE-Nluc (mABE-Nluc) to better approximate the therapeutic payload. We conducted a two-round optimization using the DoE approach described above (Supplementary Tables 1 and 2), revealing distinct formulation preferences based on mRNA size: C12 was optimal for mABE-Nluc, whereas C1 performed best for mFluc (Fig. 2g and Supplementary Fig. 18). This divergence underscores the necessity of selecting size-matched reporter mRNA during LNP formulation screening to ensure accurate optimization. In vivo validation confirmed the superior transfection efficiency of C12 in mouse lungs compared with C1 for delivering mABE-Nluc (Supplementary Fig. 19). Based on these findings, C12 was selected for subsequent experiments with Cas9 mRNA (mCas9) and mABE, ensuring optimal LNP performance for gene-editing applications.

To evaluate the efficacy of CHCha-10 LNPs for in vivo gene editing, we encapsulated mCas9 and sgTOM sgRNA[39] (LNP-mCas9/sgTOM) and administered them intratracheally to Ai9 mice (Fig. 5a and Supplementary Fig. 20). Flow cytometry analysis revealed preferential editing of lung epithelial cells (~15.8%) with minimal off-target editing in immune (~1.3%) and endothelial (~0.35%) cells (Fig. 5b,c). Among epithelial subtypes, editing efficiencies were 6.3% in club cells, 6.4% in ciliated cells, 11.2% in basal cells and 19.4% in ionocytes (Supplementary Figs. 20 and 21). Immunofluorescence analysis further

https://doi.org/10.1038/s41563-026-02555-0

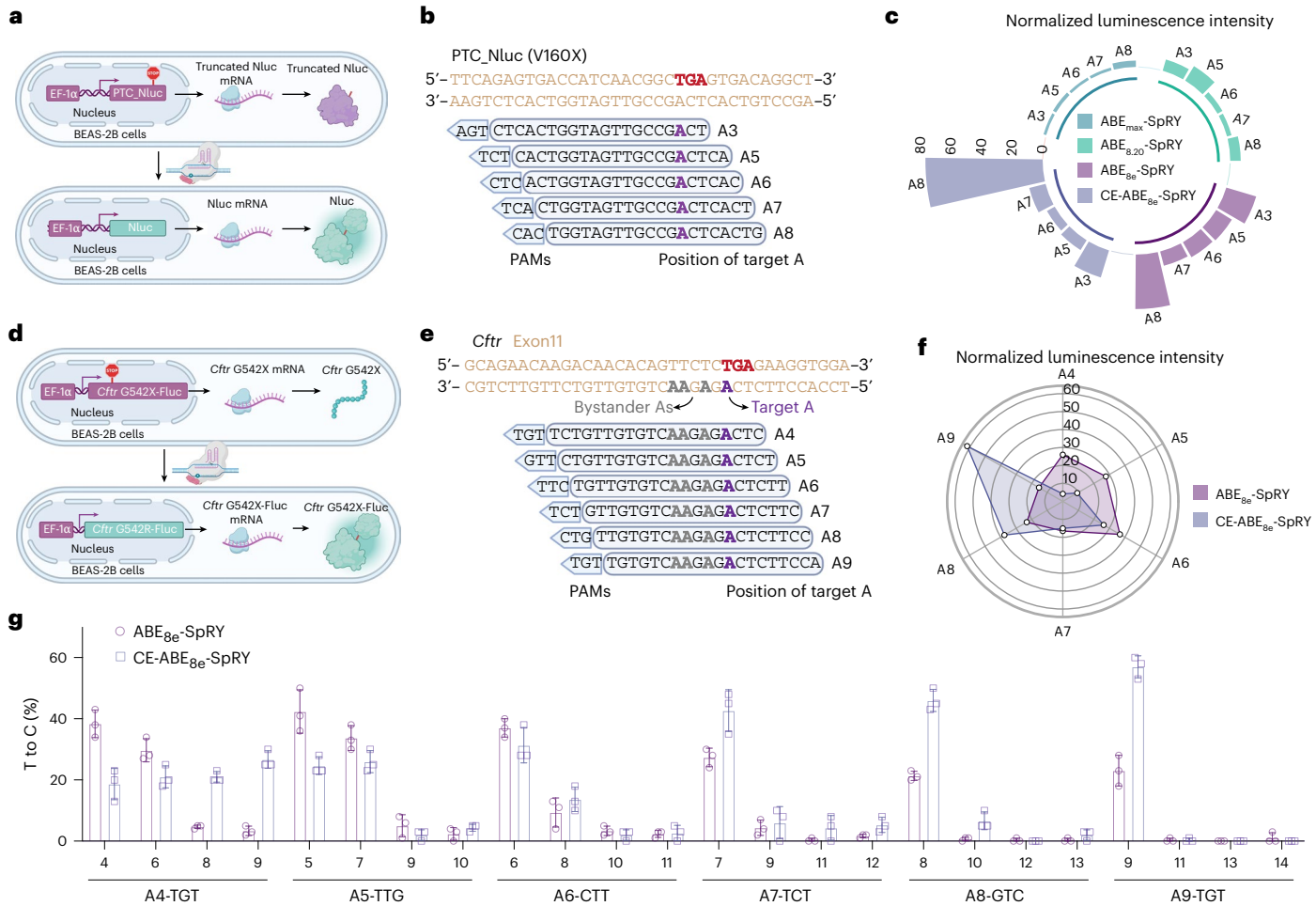


**Fig. 4 | Optimization of the ABE system to correct *Cftr* G542X. a**,**d**, Schematics of the PTC_Nluc BEAS-2B cell line (**a**) and the *Cftr* G542X_Fluc BEAS-2B cell line (**d**), depicting reporter cells before and after treatment with ABEs. **b**,**e**, A schematic of the PTC_Nluc (**b**) and *Cftr* G542X (**e**) genes with different sgRNA target sites. **c**, Normalized luminescence intensity of Nluc, relative to untreated groups, in PTC_Nluc BEAS-2B cells treated with different ABE plasmids combined with five different sgRNA expression plasmids ($n = 8$, ABE:sgRNA of 3:1, total plasmid concentration of 2 ng μl$^{-1}$). **f**,**g**, Normalized luminescence intensity of Fluc (**f**) and T-to-C editing efficiency (**g**) in *Cftr* G542X_Fluc BEAS-2B cells treated with different mABE combined with six different sgRNAs (mABE:sgRNA of 1:1, total RNA concentration of 1.5 ng μl$^{-1}$). Data in **f** are from $n = 6$ biologically independent samples. The data in **g** are from $n = 3$ biologically independent samples. The data are presented as mean values ± s.d. in **g**. Schematics created in BioRender: **a**, Li, B. https://biorender.com/jhc75b1 (2026); **b**, Li, B. https://biorender.com/w1aaz9e (2026); **d**, Li, B. https://biorender.com/20qqwf1 (2026); **e**, Li, B. https://biorender.com/l52jouu (2026).

confirmed efficient editing in club, ciliated and basal cells across both proximal and distal airways (Fig. 5d). Both inhaled CHCha-10 LNPs and intravenously administered SORT LNPs achieved 15–20% Cas9 editing in lung epithelial cells[62]. However, SORT LNPs induced substantial off-target editing in endothelial cells (~30%) and immune cells (~5%), whereas CHCha-10 LNPs exhibited minimal off-target effects in endothelial (0.3%) and immune cells (1.3%), thereby mitigating the risk of chromosomal rearrangements and potential off-target toxicity[62,63].

To demonstrate the ability of CHCha-10 LNPs to mediate in vivo base editing, we encapsulated mABE and sgFluc sgRNA into CHCha-10 LNPs (LNP-mABE/sgFluc) and administered them intratracheally to LumA mice; a luciferase reporter model carrying the R387X nonsense mutation (c.A1159T) in the Rosa26 locus[64] (Supplementary Fig. 22a). This mutation abolishes luciferase activity but can be restored upon A-to-G correction by ABE. IVIS imaging showed that intratracheal administrations of LNP-mABE/sgFluc resulted in a tenfold increase in luminescence signal in the mouse lungs (Supplementary Fig. 22b), demonstrating efficient pulmonary base editing in LumA mice.

Next, the efficacy of base editing enabled by CHCha-10 LNPs to restore CFTR expression and functionality in HBE cells carrying the *CFTR* G542X mutation was evaluated. CFTR_A9 sgRNA, prepared following the optimized sgRNA design principles aforementioned, was loaded with mABE into CHCha-10 LNPs (LNP-mABE/A9, 1:1 mABE:sgRNA ratio, total RNA 3 ng μl$^{-1}$), which were then added to HBE cells with *CFTR* G542X (Fig. 5e). Sanger sequencing showed 24.7% on-target T-to-C editing efficiency with no detectable bystander editing (Fig. 5f,g). Functional recovery of CFTR protein activity was confirmed using a fluorescence imaging plate reader (FLIPR) assay to measure chloride ion ($Cl^-$) efflux[65]. Treated cells exhibited markedly enhanced $Cl^-$ efflux upon forskolin stimulation, with levels comparable to those of wild-type (WT) HBE cells (Fig. 5h). The maximum relative fluorescence intensity ($F_{max}$) minus the baseline intensity ($F_0$) reflected CFTR activity, with treated cells demonstrating markedly higher CFTR function than untreated cells and no statistical difference compared with the healthy control HBE WT group (Fig. 5i). Western blot and RT–qPCR analyses confirmed restored CFTR protein (48%) and mRNA expression (67%) relative to WT levels (Fig. 5j,k).

The therapeutic efficacy of LNP-mABE/A9 was also evaluated in vivo using the homozygous B6-Tg(G542X)Cwr CF mouse model (G542X mouse model)[66] (Fig. 5l). Intratracheal administration of LNP-mABE/A9 (0.75 mg kg$^{-1}$) achieved approximately 12% editing efficiency in bulk lung tissue (Fig. 5m). Efficient on-target T-to-C editing was

https://doi.org/10.1038/s41563-026-02555-0

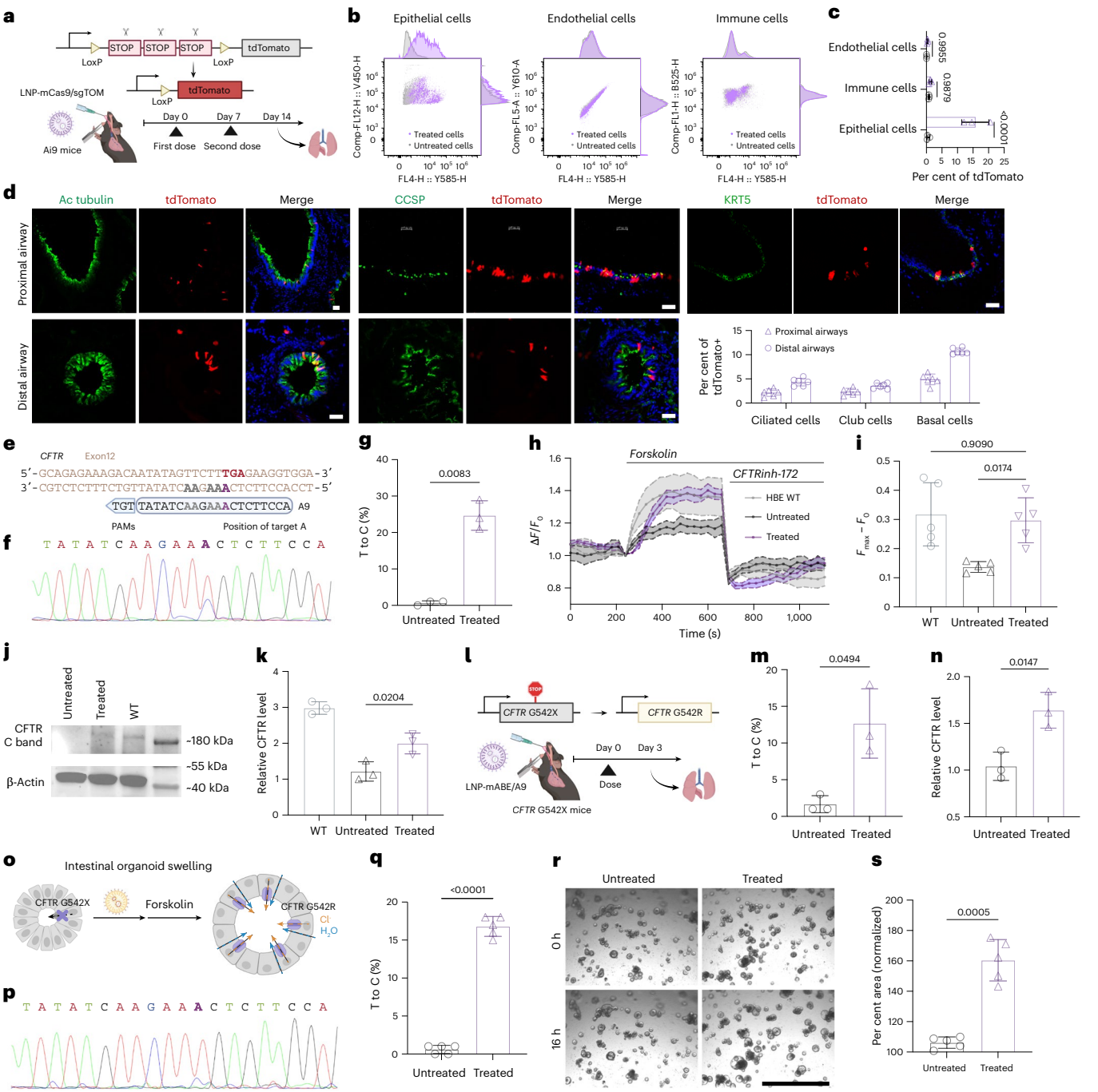


**Fig. 5 | CHCha-10 LNPs enable ABE-mediated CFTR G542X correction in vitro and in vivo. a**, A schematic of the experimental procedure for assessing LNP-mCas9/sgTOM editing efficiency in Ai9 reporter mice. Mice treated with PBS served as untreated controls. **b**, A uniform manifold approximation and projection showing the proportion of tdTomato-positive lung cells. **c**, Flow cytometry analysis quantifying the percentage of the tdTomato-positive lung cells ($n = 3$, ordinary two-way analysis of variance (ANOVA), $P = 0.0000007546$). **d**, Representative immunofluorescence images of lung sections from treated Ai9 reporter mice. Scale bar, 50 µm. A quantification of colocalization signals between tdTomato-positive cells and different subtypes of lung epithelial cells ($n = 6$ images per region, $n = 3$ biologically independent samples). **e**, A schematic of the *CFTR* G542X locus showing the sgRNA target site for the base editor. **f**,**g**, DNA sequencing results (**f**) and quantitative T-to-C editing efficiency (**g**) of treated HBE G542X cells. Quantitative results were analysed by EditR ($n = 3$). **h**, Relative fluorescence signals of treated HBE G542X cells in response to forskolin (10 µM) and CFTRinh-172 (10 µM), measured by FLIPR assay ($n = 5$). **i**, Maximum forskolin-induced fluorescence signal change ($n = 5$, ordinary one-way ANOVA). **j**,**k**, Western blot (**j**) and RT–qPCR (**k**) analyses evaluating CFTR level in treated HBE G542X cells ($n = 3$). **l**, Schematic of the experimental procedure for assessing editing efficiency in G542X disease mice. **m**,**n**, DNA sequencing results (**m**) and RT–qPCR quantification (**n**) of treated G542X mouse lungs ($n = 3$, unpaired *t*-test with Welch's correction). **o**, A schematic illustrating the intestinal organoid-based forskolin-induced swelling assay. **p**,**q**, DNA sequencing results (**p**) and quantitative T-to-C editing efficiency (**q**) in treated intestinal organoids ($n = 5$, unpaired *t*-test with Welch's correction, $P = 0.00000080501$). **r**,**s**, Images (**r**) and quantitative analyses (**s**) of intestinal organoid swelling ($n = 5$, unpaired *t*-test with Welch's correction). Scale bar, 1 mm. Percentage area changes were normalized to 0 h and quantified using ImageJ. Data are presented as mean values ± s.d. in **c**, **g**, **i**, **m**, **n**, **q** and **s**. Schematics created in BioRender: **a**, Li, B. https://biorender.com/juioj6f (2026); **e**, Li, B. https://biorender.com/r0ts4aw (2026); **l**, Li, B. https://biorender.com/7gyoaj0 (2026); **o**, Li, B. https://biorender.com/t2en1zt (2026).

further confirmed by amplicon sequencing (Supplementary Fig. 23), which led to approximately 50% increase in *CFTR* mRNA levels compared with untreated controls (Fig. 5n). Moreover, immunofluorescence staining confirmed successful restoration of CFTR protein expression in the lungs of G542X mice treated with LNP-mABE/A9, whereas no CFTR signal was detected in lungs from untreated mice (Supplementary Fig. 24).

Although the CF mouse model carries the CFTR G542X nonsense mutation, its lung tissues do not exhibit CF-related pathology[66]. To further evaluate the therapeutic potential of our approach in correcting the CFTR defect, we leveraged intestinal organoids derived from G542X mouse intestinal stem cells as an ex vivo model. This system enables functional assessment of CFTR channel restoration following treatment with LNP-mABE/A9, providing a physiologically relevant platform to validate ABE-mediated recovery of CFTR activity[66]. Functional CFTR channels facilitate ion and water transport, leading to organoid swelling upon forskolin stimulation (Fig. 5o). EditR analysis confirmed a 16.8% T-to-C editing efficiency in treated G542X organoids, with no detectable bystander mutations (Fig. 5p,q). Following treatment, forskolin stimulation induced robust organoid swelling (Fig. 5r), and quantitative analysis at 16 h post treatment revealed a 160% increase in swelling, indicating restoration of functional CFTR protein (Fig. 5s). These findings establish CHCha-10 LNPs as an effective vehicle to deliver therapeutic base editors for gene correction.

## Outlook

Efficient in vivo delivery of gene-editing tools to the lungs represents a major challenge in advancing therapies for genetic pulmonary diseases. This study addresses this challenge by introducing CHCha-10, a newly designed amino acid-derived biocompatible ionizable lipid identified through high-throughput screening, for facilitating mRNA delivery to lung epithelial cells via inhalation. Although CHCha-10 LNPs exhibit robust efficacy and biocompatibility, clinical translation requires long-term safety and immunogenicity studies in large animals, optimization of nebulization stability for current formulations and validation of delivery for other *CFTR* mutations and emerging editors such as prime editors. Overall, this study establishes inhalable CHCha-10 LNPs as a non-viral platform for the pulmonary delivery of RNA-based therapeutics, represents a promising step towards advancing gene-editing tools for treating genetic pulmonary diseases.

## Online content

Any methods, additional references, Nature Portfolio reporting summaries, source data, extended data, supplementary information, acknowledgements, peer review information; details of author contributions and competing interests; and statements of data and code availability are available at https://doi.org/10.1038/s41563-026-02555-0.

## References


1. Cullot, G. et al. CRISPR–Cas9 genome editing induces megabase-scale chromosomal truncations. *Nat. Commun.* **10**, 1136 (2019).
2. Porto, E. M., Komor, A. C., Slaymaker, I. M. & Yeo, G. W. Base editing: advances and therapeutic opportunities. *Nat. Rev. Drug Discov.* **19**, 839–859 (2020).
3. Gaudelli, N. M. et al. Programmable base editing of A*T to G*C in genomic DNA without DNA cleavage. *Nature* **551**, 464–471 (2017).
4. Musunuru, K. et al. Patient-specific in vivo gene editing to treat a rare genetic disease. *N. Engl. J. Med.* **392**, 2235–2243 (2025).
5. Davis, J. R. et al. Efficient in vivo base editing via single adeno-associated viruses with size-optimized genomes encoding compact adenine base editors. *Nat. Biomed. Eng.* **6**, 1272–1283 (2022).
6. Zhang, H. et al. Adenine base editing in vivo with a single adeno-associated virus vector. *GEN Biotechnol.* **1**, 285–299 (2022).
7. Kim, D. Y. et al. Hypercompact adenine base editors based on transposase B guided by engineered RNA. *Nat. Chem. Biol.* **18**, 1005–1013 (2022).
8. Levy, J. M. et al. Cytosine and adenine base editing of the brain, liver, retina, heart and skeletal muscle of mice via adeno-associated viruses. *Nat. Biomed. Eng.* **4**, 97–110 (2020).
9. Xu, L. et al. Efficient precise in vivo base editing in adult dystrophic mice. *Nat. Commun.* **12**, 3719 (2021).
10. Koblan, L. W. et al. In vivo base editing rescues Hutchinson–Gilford progeria syndrome in mice. *Nature* **589**, 608–614 (2021).
11. Choi, E. H. et al. In vivo base editing rescues cone photoreceptors in a mouse model of early-onset inherited retinal degeneration. *Nat. Commun.* **13**, 1830 (2022).
12. Cui, C. et al. A base editor for the long-term restoration of auditory function in mice with recessive profound deafness. *Nat. Biomed. Eng.* **9**, 40–56 (2024).
13. Guo, C., Ma, X., Gao, F. & Guo, Y. Off-target effects in CRISPR/Cas9 gene editing. *Front. Bioeng. Biotechnol.* **11**, 1143157 (2023).
14. Brommel, C. M., Cooney, A. L. & Sinn, P. L. Adeno-associated virus-based gene therapy for lifelong correction of genetic disease. *Hum. Gene Ther.* **31**, 985–995 (2020).
15. Mingozzi, F. & High, K. A. Immune responses to AAV vectors: overcoming barriers to successful gene therapy. *Blood* **122**, 23–36 (2013).
16. Musunuru, K. et al. In vivo CRISPR base editing of PCSK9 durably lowers cholesterol in primates. *Nature* **593**, 429–434 (2021).
17. Rothgangl, T. et al. In vivo adenine base editing of PCSK9 in macaques reduces LDL cholesterol levels. *Nat. Biotechnol.* **39**, 949–957 (2021).
18. Qiu, M. et al. Lipid nanoparticle-mediated codelivery of Cas9 mRNA and single-guide RNA achieves liver-specific in vivo genome editing of Angptl3. *Proc. Natl Acad. Sci. USA* **118**, e2020401118 (2021).
19. Song, C. Q. et al. Adenine base editing in an adult mouse model of tyrosinaemia. *Nat. Biomed. Eng.* **4**, 125–130 (2020).
20. Jiang, T. et al. Chemical modifications of adenine base editor mRNA and guide RNA expand its application scope. *Nat. Commun.* **11**, 1979 (2020).
21. Turuvekere Vittala Murthy, N., Vlasova, K., Renner, J., Jozic, A. & Sahay, G. A new era of targeting cystic fibrosis with non-viral delivery of genomic medicines. *Adv. Drug Deliv. Rev.* **209**, 115305 (2024).
22. Patel, M. N. et al. Safer non-viral DNA delivery using lipid nanoparticles loaded with endogenous anti-inflammatory lipids. *Nat. Biotechnol.* **44**, 79–89 (2025).
23. Witten, J. et al. Artificial intelligence-guided design of lipid nanoparticles for pulmonary gene therapy. *Nat. Biotechnol.* **43**, 1790–1799 (2024).
24. Zhao, S. et al. Acid-degradable lipid nanoparticles enhance the delivery of mRNA. *Nat. Nanotechnol.* **19**, 1702–1711 (2024).
25. Fenton, O. S. et al. Customizable lipid nanoparticle materials for the delivery of siRNAs and mRNAs. *Angew. Chem. Int. Ed. Engl.* **57**, 13582–13586 (2018).
26. Miao, L. et al. Delivery of mRNA vaccines with heterocyclic lipids increases anti-tumor efficacy by STING-mediated immune cell activation. *Nat. Biotechnol.* **37**, 1174–1185 (2019).
27. Chen, J. et al. Combinatorial design of ionizable lipid nanoparticles for muscle-selective mRNA delivery with minimized off-target effects. *Proc. Natl Acad. Sci. USA* **120**, e2309472120 (2023).
28. Xu, S. et al. Tumor-tailored ionizable lipid nanoparticles facilitate IL-12 circular RNA delivery for enhanced lung cancer immunotherapy. *Adv. Mater.* **36**, e2400307 (2024).
29. Renner, J. et al. Synthesis of ionizable lipids for gene delivery to the lung using an ugi four component reaction. *J. Am. Chem. Soc.* **147**, 17459–17467 (2025).

30. Xu, Y. et al. AGILE platform: a deep learning powered approach to accelerate LNP development for mRNA delivery. *Nat. Commun.* **15**, 6305 (2024).
31. Cornebise, M. et al. Discovery of a novel amino lipid that improves lipid nanoparticle performance through specific interactions with mRNA. *Adv. Funct. Mater.* **32**, 2106727 (2022).
32. Dong, Y. et al. Lipopeptide nanoparticles for potent and selective siRNA delivery in rodents and nonhuman primates. *Proc. Natl Acad. Sci. USA* **111**, 3955–3960 (2014).
33. Kauffman, K. J. et al. Optimization of lipid nanoparticle formulations for mRNA delivery in vivo with fractional factorial and definitive screening designs. *Nano Lett.* **15**, 7300–7306 (2015).
34. Fenton, O. S. et al. Synthesis and biological evaluation of ionizable lipid materials for the in vivo delivery of messenger RNA to B lymphocytes. *Adv. Mater.* **29**, 1606944 (2017).
35. Neve, R. L., Carrillo, B. D. & Phelan, V. V. Impact of artificial sputum medium formulation on *Pseudomonas aeruginosa* secondary metabolite production. *J. Bacteriol.* **203**, e0025021 (2021).
36. Tang, X. X. et al. Acidic pH increases airway surface liquid viscosity in cystic fibrosis. *J. Clin. Invest.* **126**, 879–891 (2016).
37. Guo, Y. et al. Mucus penetration of surface-engineered nanoparticles in various pH microenvironments. *ACS Nano* **17**, 2813–2828 (2023).
38. Billingsley, M. M. et al. Orthogonal design of experiments for optimization of lipid nanoparticles for mRNA engineering of CAR T cells. *Nano Lett.* **22**, 533–542 (2022).
39. Li, B. et al. Combinatorial design of nanoparticles for pulmonary mRNA delivery and genome editing. *Nat. Biotechnol.* **41**, 1410–1415 (2023).
40. Kauffman, K. J. et al. Rapid, single-cell analysis and discovery of vectored mRNA transfection in vivo with a loxP-flanked td Tomato reporter mouse. *Mol. Ther. Nucleic Acids* **10**, 55–63 (2018).
41. Zhang, W. et al. Lipid carriers for mRNA delivery. *Acta Pharm. Sin. B* **13**, 4105–4126 (2023).
42. Patel, S. et al. Naturally-occurring cholesterol analogues in lipid nanoparticles induce polymorphic shape and enhance intracellular delivery of mRNA. *Nat. Commun.* **11**, 983 (2020).
43. Liu, S. et al. Charge-assisted stabilization of lipid nanoparticles enables inhaled mRNA delivery for mucosal vaccination. *Nat. Commun.* **15**, 9471 (2024).
44. Ha, J. G. & Cho, H. J. Unraveling the role of epithelial cells in the development of chronic rhinosinusitis. *Int. J. Mol. Sci.* **24**, 14229 (2023).
45. Tummler, B. Progress in understanding the molecular pathology and microbiology of cystic fibrosis. *Lancet Respir. Med.* **8**, 8–10 (2020).
46. Sun, Y. et al. In vivo editing of lung stem cells for durable gene correction in mice. *Science* **384**, 1196–1202 (2024).
47. Shah, V. S. & Rajagopal, J. Cystic fibrosis: 'ionocyte modulators'?. *Am. J. Respir. Cell Mol. Biol.* **69**, 250–252 (2023).
48. Hewitt, R. J. & Lloyd, C. M. Regulation of immune responses by the airway epithelial cell landscape. *Nat. Rev. Immunol.* **21**, 347–362 (2021).
49. Rosen, B. H. et al. Animal and model systems for studying cystic fibrosis. *J. Cyst Fibros.* **17**, S28–S34 (2018).
50. Sun, X. et al. Disease phenotype of a ferret CFTR-knockout model of cystic fibrosis. *J. Clin. Invest.* **120**, 3149–3160 (2010).
51. Yu, M. et al. Highly efficient transgenesis in ferrets using CRISPR/Cas9-mediated homology-independent insertion at the ROSA26 locus. *Sci. Rep.* **9**, 1971 (2019).
52. Luo, M. et al. Genome editing in ferret airway epithelia mediated by CRISPR/nucleases delivered with amphiphilic shuttle peptides. *Hum. Gene Ther.* **34**, 705–718 (2023).
53. Carraro, G. & Stripp, B. R. Roles for myoepithelial cells in the formation and maintenance of submucosal glands. *Am. J. Respir. Cell Mol. Biol.* **56**, 685–686 (2017).
54. Fiumara, M. et al. Genotoxic effects of base and prime editing in human hematopoietic stem cells. *Nat. Biotechnol.* **42**, 877–891 (2024).
55. Walton, R. T., Christie, K. A., Whittaker, M. N. & Kleinstiver, B. P. Unconstrained genome targeting with near-PAMless engineered CRISPR–Cas9 variants. *Science* **368**, 290–296 (2020).
56. Lueck, J. D. et al. Engineered transfer RNAs for suppression of premature termination codons. *Nat. Commun.* **10**, 822 (2019).
57. Albers, S. et al. Engineered tRNAs suppress nonsense mutations in cells and in vivo. *Nature* **618**, 842–848 (2023).
58. Alves, C. R. R. et al. Optimization of base editors for the functional correction of SMN2 as a treatment for spinal muscular atrophy. *Nat. Biomed. Eng.* **8**, 118–131 (2024).
59. Cao, X. et al. Engineering of near-PAMless adenine base editor with enhanced editing activity and reduced off-target. *Mol. Ther. Nucleic Acids* **28**, 732–742 (2022).
60. Gaudelli, N. M. et al. Directed evolution of adenine base editors with increased activity and therapeutic application. *Nat. Biotechnol.* **38**, 892–900 (2020).
61. Ly, H. H., Daniel, S., Soriano, S. K. V., Kis, Z. & Blakney, A. K. Optimization of lipid nanoparticles for saRNA expression and cellular activation using a design-of-experiment approach. *Mol. Pharm.* **19**, 1892–1905 (2022).
62. Wei, T. et al. Lung SORT LNPs enable precise homology-directed repair mediated CRISPR/Cas genome correction in cystic fibrosis models. *Nat. Commun.* **14**, 7322 (2023).
63. Lahr, W. S., Sipe, C. J., Skeate, J. G., Webber, B. R. & Moriarity, B. S. CRISPR–Cas9 base editors and their current role in human therapeutics. *Cytotherapy* **25**, 270–276 (2023).
64. Yu, S. Y. et al. A luciferase reporter mouse model to optimize in vivo gene editing validated by lipid nanoparticle delivery of adenine base editors. *Mol. Ther.* **31**, 1159–1166 (2023).
65. Molinski, S. V., Ahmadi, S., Hung, M. & Bear, C. E. Facilitating structure–function studies of CFTR modulator sites with efficiencies in mutagenesis and functional screening. *J. Biomol. Screen.* **20**, 1204–1217 (2015).
66. McHugh, D. R. et al. A G542X cystic fibrosis mouse model for examining nonsense mutation directed therapies. *PLoS ONE* **13**, e0199573 (2018).

[1]Leslie Dan Faculty of Pharmacy, University of Toronto, Toronto, Ontario, Canada. [2]Institute of Biomedical Engineering, University of Toronto, Toronto, Ontario, Canada. [3]Department of Pharmacology and Toxicology, University of Toronto, Toronto, Ontario, Canada. [4]Department of Chemistry, University of Toronto, Toronto, Ontario, Canada. [5]Department of Anatomy and Cell Biology, Carver College of Medicine, University of Iowa, Iowa, IA, USA. [6]Division of Pulmonary, Allergy and Critical Care Medicine, Department of Medicine, University of Alabama at Birmingham, Birmingham, AL, USA. [7]Translational Medicine Program, Hospital for Sick Children Research Institute, Toronto, Ontario, Canada. [8]Department of Laboratory Medicine and Pathobiology, University of Toronto, Toronto, Ontario, Canada. [9]Program in Developmental and Stem Cell Biology, Hospital for Sick Children, Toronto, Ontario, Canada. [10]Michael Smith Laboratories, University of British Columbia, Vancouver, British Columbia, Canada. [11]Department of Genetics and Genome Sciences, Case Western Reserve University School of Medicine, Cleveland, OH, USA. [12]Department of Pediatrics, Case Western Reserve University School of Medicine, Cleveland, OH, USA. [13]Princess Margaret Cancer Center, University Health Network, Toronto, Ontario, Canada. [14]These authors contributed equally: Fanglin Gong, Yue Xu. ✉e-mail: bw.li@utoronto.ca

## Methods

All animal studies were approved and conducted in compliance with the University Health Network Animal Resources Centre guidelines (AUP#: 6842 and AUP#: 6856).

### Plasmid constructs

$ABE_{max}$-SpRY (Addgene, cat. no. 140003), $ABE_{8.20}$-SpRY (Addgene, cat. no. 185917) and pGL3-U6-sgRNA-EGFP (Addgene, cat. no. 107721) were purchased from Addgene. $ABE_{8e}$-SpRY (Addgene, cat. no. 185912) and CE-$ABE_{8e}$-SpRY (Addgene, cat. no. 188913) were cloned into the in vitro transcription (IVT) template vector (T7 promoter combined with 5′UTR (5′-GGGACATCGTAGAGAGTCGTACTTAGAAAAATCTATAGCAGAAGTCAGCGGTAGACGCACGGCATAGCATCCAAC-3′) and 3′UTR (5′-CAAGCACGCAGCAATGCAGCTCAAAACGCTTAGCCTAGCCACACCCCCACGGGAAACAGCAGTGATTAACCTTTAGCAATAAACGTTTAACTAAGCTATACTAACCCCAGGGTTGGTCAATTTCGTGCCAGCCACACCGAAA-3′)), using the NEBuilder HiFi DNA Assembly Cloning Kit (NEB, cat. no.E5520). P2A-Nluc fragment was ordered from gBlock Gene Fragments (Integrated DNA Technologies) and cloned into CE-$ABE_{8e}$-SpRY IVT template vector using the NEBuilder HiFi DNA Assembly Cloning Kit. To evaluate the sgRNA for correcting the *Cftr* G542X mutation in mice, we employed PB_PTC_Nluc and PB_*Cftr* G542X_Fluc PiggyBac systems. Stop codon TGA was inserted into Nluc within pB-EF1a-Nluc-IRES-Puro (Addgene #130936), resulting in pB-EF1a-Nluc V160X-IRES-Puro (PB_PTC_Nluc). A 45-nucleotide stretch from the *Cftr* G542X gene, containing premature termination codon mutations combined with Fluc (*Cftr* G542X_Fluc), was inserted into the pB-EF1a-Nluc-IRES-Puro plasmid, where the Nluc gene was replaced with *Cftr* G542X_Fluc, resulting in the PB_*Cftr* G542X_Fluc. The *Cftr* G542X-Fluc fragment was purchased from Integrated DNA Technologies' gBlock Gene Fragments. All constructs were transformed into 10-beta Competent cells (NEB, cat. no. C3019) and stored as glycerol stocks at −80 °C. For subsequent experiments and mammalian assays, purified vectors were obtained using the PureYield Plasmid Miniprep (Promega, cat. no. A1222), which includes an endotoxin removal step. Antibiotics for plasmid maintenance and selection during experiments were purchased from Invivogen. All plasmid sequences were validated by whole-plasmid sequencing (Plasmidsaurus).

### Cell culture

Human lung epithelial BEAS-2B cells (ATCC, cat. no. CRL-3588), 16HBE14o- (Sigma, cat. no. SCC150, HBE) cells and CFF-16HBEge CFTR G542X cells (HBE G542X cells, a gift from Dr Hillary Valley and the Cystic Fibrosis Foundation Therapeutic Lab) were maintained in Eagle's Minimum Essential Medium supplemented with 10% fetal bovine serum (Gibco) and 1% penicillin–streptomycin (Gibco). Primary ferret airway basal cells were kindly provided by Dr Ziying Yan, Dr Yinghua Tang and Dr John F. Engelhardt from the University of Iowa.

### BEAS-2B reporter cell construct

To construct the reporter cell line, BEAS-2B cells were seeded in a 6-well plate at a density of $1 \times 10^6$ cells per well. The cells were then transfected with FuGENE6 at 3 µl to 1 µg (transfection reagent to DNA ratio) as recommended by the manufacturer. One µg of DNA contains 0.2 µg of super PiggyBac transposase vector (System Biosciences) and 0.6 µg of PB_PTC_Nluc or PB_*Cftr* G542X_Fluc. Three days after transfection, supernatant culture media was replaced with culture media supplemented with 2 µg $ml^{-1}$ puromycin selection reagent (InvivoGen, cat. no. 58-58-2). After incubating for 24 h with puromycin, cells were washed with PBS twice and supplied with new culture media. Surviving cells were designated as PTC_Nluc BEAS-2B reporter cells or *Cftr* G542X_Fluc BEAS-2B reporter cells, respectively.

### mRNA synthesis and sgRNA

$ABE_{8e}$-SpRY, CE-$ABE_{8e}$-SpRY and CE-$ABE_{8e}$-SpRY-Nluc mRNAs were synthesized by linearizing ABE plasmids using NdeI (NEB, cat. no. R0111), cleaning with the FastPure Gel DNA Extraction Kit (Vazyme, cat. no. DC301), and conducting IVT with the HiScribe T7 RNA Synthesis Kit (NEB, cat. no. E2040), substituting $N^1$-methyl-pseudouridine-5′-triphosphate (SyngeneBio) for UTP. The IVT product was precipitated using 3.75 M lithium chloride, incubated at −20 °C and pelleted by centrifugation at 17,000*g* for 20 min at 4 °C. The pellet was washed once with ice-cold 70% ethanol, air dried and resuspended in nuclease-free water. mRNA was capped with the Faustovirus capping enzyme (NEB, cat. no. M2081) and 2′-*O*-methyltransferase (NEB, cat. no. M0366), followed by poly(A) tailing with *E. coli* poly(A) polymerase (NEB, cat. no. M0276). The product was purified, quantified by NanoDrop and diluted to 1 µg $µl^{-1}$ for LNP encapsulation. The sgRNA was chemically modified with 2′-*O*-methylation and phosphorothioate bonds in or between the first three and last three nucleotides and sourced from IDT (Supplementary Table 3).

### ABEs and sgRNA optimization in BEAS-2B reporter cells

For cell-based studies, BEAS-2B reporter cells were seeded in either 96-well or 24-well plates at densities of $1 \times 10^4$ or $1 \times 10^5$ cells per well, respectively. mABEs and sgRNA (3:1 w/w for plasmids, 1:1 w/w for mRNA) were delivered by Lipofectamine 2000 (Fig. 4c) and Lipofectamine MessagerMax (Fig. 4f). Two days later, fresh medium was added to each well to ensure adequate nutrition. After 3 days of treatment, bioluminescence from cells in the 96-well plates was measured using the Nano-Glo reagent (Promega, cat. no. N1120) and quantified using a plate reader (Citation5). For the 24-well plates, genomic DNA was extracted using the DNeasy Blood & Tissue Kit (QIAGEN, cat. no. 69504) and amplified using PCR. PCR amplicons were purified using the Wizard SV Gel and PCR Clean-Up System (Promega, cat. no. A9282) and sequenced by the TCAG DNA Sequencing Facility at SickKids. Sequencing data were analysed using EditR[67,68] to calculate editing efficiency. For cells cultured in 24-well plates, total RNA was extracted using TRIzol reagent (Thermo Fisher, cat. no. 15596026) and purified with the Direct-zol RNA MiniPrep Kit (Zymo, cat. no. R2050). RT–qPCR was performed using primers listed in Supplementary Table 4 and the Luna Universal One-Step RT–qPCR Kit (New England Biolabs, cat. no. E3005). All reactions were carried out in 384-well plates on a CFX Opus 384 real-time PCR system (Bio-Rad).

### Ionizable lipid library synthesis

Amino acids, alcohols and isocyanides were purchased from Sigma-Aldrich and Tokyo Chemical Industry (TCI). Ester bonds in the tail chains were synthesized through an esterification reaction between 1,6-diols and the corresponding carboxylic acid chains[28]. Meanwhile, fatty chains with primary alcohol groups lacking ester bonds were selectively oxidized to aldehydes using Dess–Martin periodinane reagents, following previously published methods[69]. High-throughput synthesis of amino acid-derived lipids was performed in 96-well PCR plates at a 2:2:1 molar ratio of amino acid, aldehyde and isocyanide. The reactions proceeded in methanol at room temperature for 24 h with an acceptable conversion yield[70–72]. The crude product underwent further purification using silica gel column chromatography (BUCHI) using hexane/ethyl acetate or DCM/methanol as the eluent for subsequent analysis.

### Preparation of LNPs

For high-throughput screening, LNPs were formulated by an automated OT-2 liquid handler, as described in our previous work[30]. For non-high-throughput screening preparations, LNPs were formed by mixing the aqueous mRNA solution with the lipid–ethanol phase either manually (for volumes <100 µl) or via a T-junction microfluidic device (for volumes >100 µl). The aqueous phase comprised 10 mM citrate buffer containing mFluc (TriLink, cat. no. L-7602), mCre (TriLink, cat. no. L-7603), in-house synthesized mABE mRNA or sgRNA (IDT, Alt-R CRISPR–Cas9 sgRNA). The ethanol phase

contained ionizable lipids, helper phospholipids (DOTAP; Avanti, cat. no. 890890P; DOPE; Avanti, cat. no. 850725 P; DPPC; Avanti, cat. no. 850355P; and DSPC; Avanti, cat. no. 850365P), cholesterol (Sigma-Aldrich, cat. no. C8667), β-sitosterol (ApexBio, cat. no. B6199), stigmasterol (Cayman, cat. no. 10011326) and C14-PEG2000 (Avanti, cat. no. 880150P) at predetermined molar ratios, typically with an ionizable lipid:mRNA weight ratio of 10:1. For LNPs prepared via the T-junction method, the aqueous and ethanol phases were mixed in a microfluidic device at a 3:1 ratio using syringe pumps, resulting in a final mRNA concentration of 0.1 mg ml$^{-1}$ for in vitro experiments. LNPs were dialysed against PBS overnight at 4 °C using 100 kDa molecular weight cut-off Spectra/Por cassettes (Thermo Fisher, cat. no. 132670), and then concentrated via centrifugation in 100 kDa molecular weight cut-off Amicon Ultra-0.5 filters (Millipore, cat. no. UFC510096). For pipette-mixed LNPs, the aqueous and ethanol phases were mixed manually through repeated pipetting.

### ALI culture

ALI-differentiated primary ferret basal epithelial cells were kindly provided by Dr Jim Hu, Dr Zhichang Peter Zhou and Ziyan Chen (SickKids Research Institute). The differentiation of BEAS-2B cells[73] or primary ferret airway epithelial cells in ALI culture followed STEMCELL protocol. In brief, $3.3 \times 10^4$ BEAS-2B cells or primary ferret airway epithelial cells were seeded in the 6.5-mm Transwell insert with 0.2 ml PneumaCult complete base medium (STEMCELL Technologies). After 3 days of expansion, the media in the insert was aspirated and 0.5 ml PneumaCult complete base medium in the basal chamber was replaced by 0.5 ml PneumaCult maintenance media (STEMCELL Technologies). A full media change was performed every 2 days. After airlifting for 28 days, cells were differentiated and ready for transfection with LNPs. Before transfection, 5 µl of artificial sputum medium was applied atop differentiated BEAS-2B ALI cultures to mimic airway mucus.

### FRET assay

LNP-endosomal membrane fusion was assessed using a FRET-based assay[74]. DOPE-conjugated FRET probes NBD-PE and Rho-PE were formulated into nanoparticles of the same mimetic endosome, which resulted in diminished NBD fluorescence due to the FRET effect of rhodamine. Once lipid fusion occurs, the NBD signal increases due to the increased distance between the two probes. Endosomal mimetic nanoparticles were prepared by mixing DOPS:DOPC:DOPE:NBD-PE:Rho-PE (molar ratio 25:25:48:1:1) in chloroform, followed by rotary evaporation and then vacuum drying for 2 h to obtain a thin lipid film. The dried film was subsequently hydrated in PBS (pH 7.4), sonicated for 20 min and the total lipid concentration was fixed at 1 mM. LNPs were prepared as described above for high-throughput screening preparation. PBS (pH 5.5) was added to a black 96-well plate (100 µl per well), and then 1 µl of endosomal mimetic nanoparticles (1 mM) and 5 µl LNPs were added to each well. After incubation at 37 °C for 5 min, fluorescence measurements were performed on a microplate reader at a wavelength of excitation 465/emission 520 ($F$). Only endosomal mimic anionic liposomes in PBS were set as negative control ($F_{min}$). Probe-containing lipids incubated with Triton-X-100 solution (2 wt.%) were set as a positive control ($F_{max}$). Lipid fusion (%) was calculated as $(F - F_{min})/(F_{max} - F_{min}) \times 100\%$.

### TNS binding assay

LNP pKa values were determined via the TNS binding assay[75,76]. TNS reagent was prepared in 300 µM dimethylsulfoxide stock solution. LNPs and TNS were diluted to 75 µM and 6 µM, respectively, in approximately 93 µl of TNS buffer (20 mM boric acid, 10 mM imidazole, 10 mM sodium acetate, 10 mM glycylglycine and 25 mM sodium chloride; pH 3–10). The fluorescence was read using Cytation 5 (Biotek) (excitation 321/emission 445). Sigmoidal best-fit curves were generated in GraphPad Prism 10 to determine pKa at the pH of half-maximal fluorescence.

### Animal experiments

Animals were maintained in a specific pathogen-free facility under controlled environmental conditions (12 h light and 12 h dark cycle, 24 °C, 60% humidity) with free access to food and water at the University Health Network Animal Resources Centre. C57BL/6, B6.Cg-*Gt(ROSA)26Sor*$^{tm9(CAG\text{-}tdTomato)Hze}$/J (Ai9), and C57BL/6J-*Gt(ROSA)26Sor*$^{em1Crx}$/J (LumA) mice were sourced from the Jackson Laboratory. B6-Tg(*CFTRG542X*)Cwr (*CFTR* G542X) mice were kindly provided by Dr Craig A. Hodges from Cystic Fibrosis Mouse Models Core and Dr Amy Wong and Krista Antonio from SickKids Research Institute. ROSA$^{mTmG}$ transgenic ferrets were kindly provided by Dr Ziying Yan, Dr Yinghua Tang and Dr John F. Engelhardt from the University of Iowa. Mice and ferrets of both sexes were used in this study. They were randomized assigned into different groups.

### Bioluminescence analysis

The 6–8-week-old C57BL/6 mice were intratracheally administered with 50 µl of LNP-mFluc (0.3 mg kg$^{-1}$ mFluc, 0.12 mg ml$^{-1}$ LNP-mFluc) or LNP-mABE-Nluc (0.5 mg kg$^{-1}$ ABE-Nluc mRNA, 0.2 mg ml$^{-1}$ LNP-mABE-Nluc). A total of 6 h post dose, mice received 2 mg D-luciferin via intraperitoneally injection (0.1 g kg$^{-1}$, 10 mg ml$^{-1}$). Mice were anesthetized using 1.5% isoflurane in oxygen and were killed after 10 min. Lungs were isolated and imaged using In Vivo Imaging System (IVIS, PerkinElmer). The data were processed with Living Image Software (PerkinElmer).

### Intratracheal administration of LNPs in Ai9, C57BL/6, LumA and CFTR G542X mice

The 6–8-week-old Ai9 mice were intratracheally administrated with 50 µl of LNP-mCre (0.75 mg kg$^{-1}$ mCre, 0.3 mg ml$^{-1}$ LNP-Fluc) or LNP-mCas9/sgTOM (0.75 mg kg$^{-1}$ mCas9 and sgTOM, mCas9-to-sgTOM weight ratio is 4:1, 0.3 mg ml$^{-1}$ LNP-mCas9/sgTOM) following the dosing schematics mentioned above. A total of 7 days (treating with LNP-Cre) or 14 days (treating with LNP-mCas9/sgTOM) after first dosing, mice were killed. Lungs were collected for following flow analysis and immunofluorescent staining.

The 6–8-week-old C57BL/6 mice were intratracheally administered 50 µl of LNP-mABE (0.75 mg kg$^{-1}$ mABE; 0.3 mg ml$^{-1}$ formulation), PBS or LPS (0.25 mg kg$^{-1}$). A total of 24 h after dosing, mice were killed. Serum samples were collected from the tail vein. Mice were killed for BALF sample collection. Cytokine levels in serum and BALF were quantified by Eve Technologies.

The 6–8-week-old LumA mice were intratracheally administrated with 50 µl of LNP-mABE/sgFluc (0.75 mg kg$^{-1}$ mABE and A9, mABE-to-A9 weight ratio is 1:1, 0.3 mg ml$^{-1}$ LNP-mABE/A9) following the dosing schematics mentioned above. Eleven days after first dosing, mice were killed. Lungs were collected for analysing luminescence signal.

The 5–6-week-old *CFTR* G542X mice were intratracheally administrated with 50 µl of LNP-mABE/A9 (0.75 mg kg$^{-1}$ mABE and A9, mABE-to-A9 weight ratio is 1:1, 0.3 mg ml$^{-1}$ LNP-mABE/A9) following the dosing schematics mentioned above. Three days after the first dosing, mice were killed. Lungs were collected for analysing editing efficiency and CFTR mRNA level.

### Single-cell isolation from mouse lungs

The collected lungs and proximal airways were placed in ice-cold PBS. Tissues were minced into small pieces and transferred to a 50-ml tube with 5 ml of digestion media (DMEM, 300 U ml$^{-1}$ collagenase IV, 100 U ml$^{-1}$ DNase I)[46,77–79]. The tube was incubated at 37 °C with shaking (200 rpm) for 30 min. After incubation, the lung cell solution was filtered through a 70-µm strainer into a fresh tube, rinsed with 10 ml wash buffer (ice-cold PBS, 1% FBS) and centrifuged at 500*g* for 5 min. The supernatant was discarded, and the pellet was resuspended in 10 ml wash buffer, followed by another centrifugation step. The resulting pellet was treated with 5 ml of RBC lysis buffer (Thermo Scientific, cat. no.

00-4333-57) for 5 min at room temperature to remove red blood cells. The lysis reaction was quenched with 10 ml wash media, and the sample was spun at 500*g* for 5 min. The final cell pellet, free of red blood cells, was resuspended in 5 ml of cell staining buffer (ice-cold PBS, 1% BSA). The cells were subsequently stained with antibodies for flow cytometry.

### Antibody staining of single cells from mouse lungs and analysis by flow cytometry

Single-cell suspensions, derived from the mouse lungs and proximal airways or bulk lungs, were initially blocked with TruStain FcX blocker (BioLegend, cat. no. 101320) for a period of 15 min. After that, half of the distal airway cells were stained with Alexa Fluor 594-conjugated anti-mouse CD31 antibody (BioLegend, cat. no. 102520), FITC-conjugated anti-mouse CD45 antibody (BioLegend, cat. no. 157214), BrilliantViolet 421-conjugated anti-mouse EpCAM antibody (BioLegend, cat. no. 118225) and Zombie NIR Fixable Viability Kit (BioLegend, cat. no. 423106) at room temperature for 30 min (1 µl of each antibody or dye for $10^6$ cells in 100 ml). Another half of the distal airway cells and proximal airway cells were incubated with Zombie NIR Fixable Viability Kit. Following this, the cell pellet was washed twice with cell staining buffer to eliminate excess antibodies or dye. All the cell pellet was resuspended in 500 µl of fix/perm solution, part of the BD Fix/Perm kit (BD Bioscience, cat. no. 554714), and left on ice for 30 min. Following this, the cells were centrifuged at 500*g* for 5 min to obtain cell pellets. The pellet was then washed three times with 1× fix/perm wash buffer, before being prepared for antibody staining. Subsequently, 100 µl of the CD31, CD45, EpCAM and Zombie-stained lung cells were incubated with 1 µl of Alexa Fluor 647-conjugated anti-mouse FOXI1 antibody (NovusBio, cat. no. NBP2-70747AF647) for 30 min. A total of 100 µl of the Zombie-stained lung cells were incubated with 1 µl of Alexa Fluor-594-conjugated anti-mouse Cytokeratin 5 antibody (Santa Cruz, cat. no. sc-32721), Alexa Fluor 488-conjugated anti-mouse CCSP antibody (Santa Cruz, cat. no. sc-390313) and Alexa Fluor 647-conjugated anti-mouse acetylated tubulin antibody (Santa Cruz, cat. no. sc-23950) for 30 min. After this incubation period, the cells were washed three times with a 1× fix/perm wash buffer to remove any surplus antibodies. Finally, the cell pellet was resuspended in 100 µl of 1× fix/perm wash buffer and kept on ice until it was ready for analysis by a flow cytometer.

### Immunofluorescence staining

Mouse lung samples were fixed with 4% paraformaldehyde for 2 days at 4 °C, equilibrated in 15% sucrose for 12 h, followed by 30% sucrose for 12 h and then cryosectioned. Frozen tissue sections (10 µm) mounted on charged slides were washed three times with PBS (5 min per wash), then blocked and permeabilized by incubating with a blocking buffer (PBS with 5% BSA and 0.1% Triton-X) for 1 h. Following three PBS washes, the slides were stained for 12 h at 4 °C with either Alexa Fluor 488-conjugated anti-mouse Cytokeratin 5 antibody (Santa Cruz, cat. no. sc-32721) and Alexa Fluor 647-conjugated anti-mouse acetylated tubulin antibody (Santa Cruz, cat. no. sc-23950), Alexa Fluor 488-conjugated anti-mouse CCSP antibody (Santa Cruz, cat. no. sc-390313) or Alexa Fluor 546-conjugated anti-mouse CFTR antibody (Santa Cruz, cat. no. sc-376683). The slides were then washed three times with PBS to remove unbound antibodies and stained with DAPI (Invitrogen, cat. no. P36931) for 15 min before imaging using the Leica TCS SP8 STED3X confocal microscope (UHN AMOF).

Differentiated primary ferret epithelial cells in inserts were cut and mounted on charged slides using Cytoseal 60 mounting media (Epredia). The inserts were fixed with 4% paraformaldehyde for 15 min at room temperature and washed three times with PBS (5 min per wash). Then, inserts were blocked and washed as previously mentioned and stained for 12 h at 4 °C with Alexa Fluor 647-conjugated anti-mouse Cytokeratin 5 antibody (Santa Cruz, cat. no. sc-32721), Alexa Fluor 647-conjugated anti-mouse acetylated tubulin antibody (Santa Cruz, cat. no. sc-23950) or Alexa Fluor 647-conjugated anti-mouse CCSP antibody (Santa Cruz, cat. no. sc-390313). The inserts were then washed and stained with DAPI as previously mentioned before performing *Z*-stack imaging using the Leica TCS SP8 STED3X confocal microscope (UHN AMOF).

### Ferret lung transfection

The experiment involved ferrets has been approved by the Institutional Animal Care and Use Committees (IACUC) of the University of Iowa. Juvenile ROSA$^{mTmG}$ ferrets (35 days old) were intratracheally sprayed with 300 µl of LNP-mCre (0.6 mg kg$^{-1}$ mCre, 0.3 mg ml$^{-1}$ LNP-mCre) by using a microsprayer aerosolizer (PennCentury, model IA-1B). A total of 14 days after transfection, ferrets were killed. Lungs were collected for following immunofluorescent staining and H&E staining. For immunofluorescent staining, ferret lung samples were fixed and cryosectioned into 10-µm sections as the same procedure for mouse lung samples. Slides were blocked and washed as previously mentioned and stained for 12 h at 4 °C with DyLight 550-conjugated anti-tdTomato antibody (Antibodies-online, cat. no. ABIN7273113) and FITC-conjugated anti-GFP antibody (Santa Cruz, cat. no. sc-9996). Slides were then washed and stained with DAPI as previously mentioned before performing slide scanning using the Zeiss AxioScan fluorescence scanner (UHN AMOF).

### Intestinal organoid collection and culture

Intestinal organoids were obtained from G542X mice as described in a prior study[66]. In brief, mice were killed. Their small intestines were removed, flushed with PBS and sliced longitudinally. Villi were scraped off with a razor blade, and the remaining tissue segments were cut into 0.5-cm pieces, suspended in 25 ml of Gentle Cell Dissociation Reagent (STEMCELL Technologies) and shaken gently for 30 min. In a sterile hood, the segments were vigorously shaken by hand for 30 s, and the supernatant was collected into a 10-cm dish. The segments were resuspended in ice-cold PBS (lacking $Mg^{2+}$ and $Ca^{2+}$) and shaken repeatedly, yielding four fractions of supernatant enriched with intestinal crypts. These fractions were filtered using a 70-µm strainer and centrifuged at 200*g* for 5 min. The pellet was resuspended in a 1:1 mix of MatriGel (Corning) and Intesticult Organoid Growth Media (STEMCELL Technologies). The resulting crypts were diluted to a concentration of 10 crypts µl$^{-1}$, and then plated into 24-well plates with 35 µl of the MatriGel-OGM mixture per well. After solidifying the gel at 37 °C for 15 min, 500 µl of OGM was added to each well, and the plates were incubated at 37 °C with 5% $CO_2$. Organoids were cultured with medium changes every 3 days and passaged every 7 days.

### Ex vivo G542X correction in intestinal organoids using LNPs

Organoids were incubated in Matrigel droplets in 12-well plates to prepare organoids for swelling experiments, and then approximately 75% fusion was achieved. The organoids were then released from the Matrigel, centrifuged and digested into single cells with Acutase (Life Technologies). After quenching Acutase with DMEM containing 10% FBS, individual stem cells ($3 \times 10^4$ cells per well) were seeded into Matrigel-coated 96-well plates and treated with LNP-mABE/A9 twice every 3 days (2.5 ng µl$^{-1}$ total nucleic acid each time). They were grown for 4–5 days until complete organoids were formed. A forskolin-induced swelling assay was performed with a final concentration of 10 µM forskolin and bright field images were captured with Cytation 5 (Biotek). The area of each organoid at 16 h, which is indicative of CFTR activity, was evaluated and normalized to the area at 0 h. Organoids only treated 10 µM forskolin were used as untreated groups. Cells were trypsinized from each well and genomic DNA was isolated using the DNaeasy Extraction Kit (Qiagen, cat. no. E1941). The G542X target sequence was PCR amplified using the Q5 High-Fidelity 2X Master Mix (NEB, cat. no. M0492) followed by Sanger sequencing.

### Sanger sequencing analysis

Cells were trypsinized from each well. Genomic DNA was extracted using the DNaeasy Extraction Kit (Qiagen, cat. no. E1941). The corrected region of the target gene was amplified by PCR using primers listed in Supplementary Tables 5 and 6, under the following conditions: an initial denaturation at 98 °C for 30 s, followed by 35 cycles: 10 s at 98 °C, 30 s at the corresponding temperature for each pair of primers, 30 s at 72 °C and a final extension at 72 °C for 2 min and incubation at 4 °C. Finally, it was extended at 72 °C for 2 min and kept at 4 °C. The PCR products were purified using the Wizard SV Gel and PCR Clean-Up System (Promega, cat. no. A9282). The purified PCR products were sequenced at SickKids TCAG DNA sequencing facility. Sequencing data were analysed using the EditR web tool[68] to assess editing efficiency.

### Statistical analyses

Statistical analyses were conducted with Prism 10 (GraphPad Software, version 10.1.1), and the results are shown as individual data points or as the mean ± standard deviation (s.d.). Data collection and analysis were not performed blind to the conditions of the experiments. No animals or data points were excluded from the analyses unless explicitly stated.

### Reporting summary

Further information on research design is available in the Nature Portfolio Reporting Summary linked to this article.

## Data availability

Data supporting the findings of this study are available within the article and its Supplementary Information. Sequencing data from amplicon NGS experiments are deposited in the NCBI SRA under accession code GSE317845. Source data are provided with this paper.

## Code availability

The code used in Fig. 1e is available via GitHub at https://github.com/bowenli-lab/AminoAcids.git and via Zenodo at https://doi.org/10.5281/zenodo.18613180 (ref. 80) with the MIT licence.

## References


67. Kluesner, M. G. et al. EditR: a method to quantify base editing from Sanger sequencing. *CRISPR J.* **1**, 239–250 (2018).
68. Kluesner, M. G., Nedveck, D. A., Lahr, W. S., Garbe, J., Abrahante, J., Webber, B. & Moriarty, B. S. EditR: a method to quantify base editing via Sanger sequencing. *The CRISPR Journal* http://moriaritylab.shinyapps.io/editr_v10/ (2018).
69. Xu, Y. et al. LUMI-lab: a foundation model-driven autonomous platform enabling discovery of ionizable lipid designs for mRNA delivery. *Cell* https://doi.org/10.1016/j.cell.2026.01.012 (2026).
70. Liu, H. & Dömling, A. One-pot synthesis of highly functionalized seleno amino acid derivatives. *Chem. Biol. Drug Des.* **74**, 302–308 (2009).
71. Tao, Y. & Tao, Y. Ugi reaction of amino acids: from facile synthesis of polypeptoids to sequence-defined macromolecules. *Macromol. Rapid Commun.* **42**, e2000515 (2021).
72. Pérez-Labrada, K. et al. Combined Ugi-4CR/CuAAC approach to triazole-based neoglycolipids. *Eur. J. Org. Chem.* **2014**, 3671–3683 (2014).
73. Stewart, C. E., Torr, E. E., Mohd Jamili, N. H., Bosquillon, C. & Sayers, I. Evaluation of differentiated human bronchial epithelial cell culture systems for asthma research. *J. Allergy* **2012**, 943982 (2012).
74. Liu, S. et al. Membrane-destabilizing ionizable phospholipids for organ-selective mRNA delivery and CRISPR–Cas gene editing. *Nat. Mater.* **20**, 701–710 (2021).
75. Zhang, J., Fan, H., Levorse, D. A. & Crocker, L. S. Ionization behavior of amino lipids for siRNA delivery: determination of ionization constants, SAR, and the impact of lipid pKa on cationic lipid-biomembrane interactions. *Langmuir* **27**, 1907–1914 (2011).
76. Carrasco, M. J. et al. Ionization and structural properties of mRNA lipid nanoparticles influence expression in intramuscular and intravascular administration. *Commun. Biol.* **4**, 956 (2021).
77. Pisu, D. & Russell, D. G. Protocol for multi-modal single-cell RNA sequencing on M. tuberculosis-infected mouse lungs. *STAR Protoc.* **4**, 102102 (2023).
78. Kang, M. H. et al. A lung tropic AAV vector improves survival in a mouse model of surfactant B deficiency. *Nat. Commun.* **11**, 3929 (2020).
79. Wong, A. P. et al. Efficient generation of functional CFTR-expressing airway epithelial cells from human pluripotent stem cells. *Nat. Protoc.* **10**, 363–381 (2015).
80. Xu, Y., Li, G. & Li, B. Amino acid-derived ionizable lipids enable inhaled base editing for therapeutic gene correction in the lung. *Zenodo* https://doi.org/10.5281/zenodo.18613180 (2026).


## Acknowledgements


We acknowledge the funding support from the GSK Chair Professorship, the Leslie Dan Faculty of Pharmacy startup fund, the Princess Margaret Cancer Center operating fund, the Connaught Fund (grant nos. 514681 and 523859), the J.P. Bickell Foundation (grant no. 515159), the Canada Research Chairs Program (grant no. CRC-2022-00575), the Canadian Institutes of Health Research (CIHR) Project Grants (grant nos. PJH-185722, PJT-190109, PJT-192011, PJT-195669 and PJT-203954), Ontario Early Researcher Awards Program (grant no. ER24-18-177), Stem Cell Network (grant no. ECR-C5R1-5), National Sanitarium Association (grant no. 522574), Cystic Fibrosis Canada (grant no. 1188219), the New Frontiers in Research Fund (grant no. NFRFE-2023-00203), the Natural Sciences and Engineering Research Council of Canada (grant no. RGPIN-2023-05124), National Institutes of Health (NIH) grants (grant nos. 1R01HL174773 to B.L. and R01 HL174593 to Z.Y.), the National Heart, Lung, and Blood Institute Federal Contract (grant no. 75N92025C00007 to J.F.E.) and Cystic Fibrosis Foundation grants (grant nos. LI23G0 and LI23I0 to B.L., HODGES19R1 to C.A.H., ENGELH21XX0 to J.F.E. and YAN23G0 to Z.Y). J.C. acknowledges support from the PRiME Fellowship and the Nanomedicine Innovation Network Doctoral Award. L.H. acknowledges the Queen Elizabeth II/F.E. Beamish Graduate Scholarships in Science and Technology. B.S. acknowledges the Ontario Graduate Scholarship. R.X.Z.L. acknowledges the Acceleration Consortium Postdoctoral Fellowship. T.T. acknowledges the Cystic Fibrosis Foundation Student Traineeship (grant no. 008475H224, Thomson) and the Ontario Graduate Scholarship. D.X.W.C. acknowledges a CIHR Canada Graduate Research Scholarship (Master's). The authors acknowledge technical support from the Centre for Pharmaceutical Oncology Flow Cytometry and Imaging facilities and the Princess Margaret Cancer Centre for access to NMR and animal facilities. Figures 1d, 2a and 4c,f were generated via Bioinformatics at https://www.bioinformatics.com.cn, an online platform for data analysis and visualization.


## Author contributions

F.G., Y.X. and B.L. conceived the study and designed the experiments. F.G., Y.X., J.C., S.Z., S.D., L.H., B.S., M.Z., R.X.Z.L., G.L., T.T., Y.T., Z.C. and K.A. performed the experiments and data analysis. F.G., Y.X. and B.L. wrote the study. F.G., A.V., D.X.W.C., J.H., Z.Y. and B.L. discussed the results and edited the paper. C.A.H., A.P.W., J.H., Z.Y., J.F.E., B.P.H. and B.L. acquired funding and supervised the project. All authors provided feedback and helped shape the research, data analysis and paper.

## Competing interests

F.G., Y.X. J.C. and B.L. have filed an invention disclosure for ionizable lipids. The other authors declare no competing interests.

## Additional information

**Supplementary information** The online version contains supplementary material available at https://doi.org/10.1038/s41563-026-02555-0.

**Correspondence and requests for materials** should be addressed to Bowen Li.

**Peer review information** *Nature Materials* thanks Yizhou Dong and Olivia Merkel for their contribution to the peer review of this work.

nature portfolio

Corresponding author(s): Bowen Li

Last updated by author(s): Jan 25, 2026

# Reporting Summary

Nature Portfolio wishes to improve the reproducibility of the work that we publish. This form provides structure for consistency and transparency in reporting. For further information on Nature Portfolio policies, see our Editorial Policies and the Editorial Policy Checklist.

## Statistics

For all statistical analyses, confirm that the following items are present in the figure legend, table legend, main text, or Methods section.

| n/a | Confirmed | |
|---|---|---|
| ☐ | ☒ | The exact sample size (*n*) for each experimental group/condition, given as a discrete number and unit of measurement |
| ☐ | ☒ | A statement on whether measurements were taken from distinct samples or whether the same sample was measured repeatedly |
| ☐ | ☒ | The statistical test(s) used AND whether they are one- or two-sided<br>*Only common tests should be described solely by name; describe more complex techniques in the Methods section.* |
| ☒ | ☐ | A description of all covariates tested |
| ☐ | ☒ | A description of any assumptions or corrections, such as tests of normality and adjustment for multiple comparisons |
| ☐ | ☒ | A full description of the statistical parameters including central tendency (e.g. means) or other basic estimates (e.g. regression coefficient) AND variation (e.g. standard deviation) or associated estimates of uncertainty (e.g. confidence intervals) |
| ☐ | ☒ | For null hypothesis testing, the test statistic (e.g. *F*, *t*, *r*) with confidence intervals, effect sizes, degrees of freedom and *P* value noted<br>*Give P values as exact values whenever suitable.* |
| ☒ | ☐ | For Bayesian analysis, information on the choice of priors and Markov chain Monte Carlo settings |
| ☒ | ☐ | For hierarchical and complex designs, identification of the appropriate level for tests and full reporting of outcomes |
| ☒ | ☐ | Estimates of effect sizes (e.g. Cohen's *d*, Pearson's *r*), indicating how they were calculated |

*Our web collection on statistics for biologists contains articles on many of the points above.*

## Software and code

Policy information about availability of computer code

| | |
|---|---|
| Data collection | Bio-Rad Image Lab Touch software was used to acquire Western blot images;<br>LAS X v5.3.0 was used to acquire confocal images;<br>Gen5 v3.12 was used to acquire in vitro luminescence data;<br>CFX Maestro Software was used to acquire rt-qpcr data;<br>Living Image v4.5.0 was used to acquire in vivo bioluminescence data;<br>CytExpert v2.6 was used to acquire flow cytometry data |
| Data analysis | GraphPad Prism v10 was used for statistical analyses.<br>FlowJo v10 was used for data plotting.<br>ChemDraw v22.0.0 was used for chemical structure visualization.<br>MestReNova v14.2.3 was used for NMR data analysis.<br>EditR v1.0.10 was used for analyzing the editing efficiency of base editors.<br>ImageJ was used for analyzing organoid swelling and confocal images.<br>Living Image v4.4 was used for bioluminescence data analysis from animals.<br>LAS X v3.7.6.25997 was used for processing confocal images.<br>Bio-Rad CFX Maestro v3.1 was used for analyzing RT-qPCR results.<br>Bio-Rad Image Lab Touch Software was used for merging Western blot images.<br>JMP v16 was used for formulation optimization. |

For manuscripts utilizing custom algorithms or software that are central to the research but not yet described in published literature, software must be made available to editors and reviewers. We strongly encourage code deposition in a community repository (e.g. GitHub). See the Nature Portfolio guidelines for submitting code & software for further information.

## Data

Policy information about availability of data

All manuscripts must include a data availability statement. This statement should provide the following information, where applicable:

- Accession codes, unique identifiers, or web links for publicly available datasets
- A description of any restrictions on data availability
- For clinical datasets or third party data, please ensure that the statement adheres to our policy

All experimental data have been included in the manuscript and supplementary information. The code used in Fig.1e is available in the Github repository (https://github.com/bowenli-lab/AminoAcids.git) with the MIT License. Sequencing data from amplicon NGS experiments are deposited in the NCBI SRA under accession GSE317845.

## Research involving human participants, their data, or biological material

Policy information about studies with human participants or human data. See also policy information about sex, gender (identity/presentation), and sexual orientation and race, ethnicity and racism.

| | |
|---|---|
| Reporting on sex and gender | No research involving human participants was done in this study |
| Reporting on race, ethnicity, or other socially relevant groupings | No research involving human participants was done in this study |
| Population characteristics | No research involving human participants was done in this study |
| Recruitment | No research involving human participants was done in this study |
| Ethics oversight | No research involving human participants was done in this study |

Note that full information on the approval of the study protocol must also be provided in the manuscript.

# Field-specific reporting

Please select the one below that is the best fit for your research. If you are not sure, read the appropriate sections before making your selection.

☒ Life sciences ☐ Behavioural & social sciences ☐ Ecological, evolutionary & environmental sciences

For a reference copy of the document with all sections, see nature.com/documents/nr-reporting-summary-flat.pdf

# Life sciences study design

All studies must disclose on these points even when the disclosure is negative.

| | |
|---|---|
| Sample size | The sample sizes chosen in this study were consistent with those commonly used and accepted in the field (see references: Nat Biotechnol (2024), https://doi.org/10.1038/s41587-024-02490-y; Nat Biotechnol 41, 1410–1415 (2023), https://doi.org/10.1038/s41587-023-01679-x; Science 384, 1196–1202 (2024), DOI:10.1126/science.adk9428). All sample sizes are specified in the figure legends and were sufficient to perform robust statistical analyses where applicable. |
| Data exclusions | No data were excluded. |
| Replication | Experiment in general were repeated to confirm the results. All attempts at replication were successful. |
| Randomization | Cells or animal were randomized by body weight and/or age. |
| Blinding | Experiments were generally blinded. |

# Reporting for specific materials, systems and methods

We require information from authors about some types of materials, experimental systems and methods used in many studies. Here, indicate whether each material, system or method listed is relevant to your study. If you are not sure if a list item applies to your research, read the appropriate section before selecting a response.

## Materials & experimental systems

| n/a | Involved in the study |
|---|---|
| ☐ | ☒ Antibodies |
| ☐ | ☒ Eukaryotic cell lines |
| ☒ | ☐ Palaeontology and archaeology |
| ☐ | ☒ Animals and other organisms |
| ☒ | ☐ Clinical data |
| ☒ | ☐ Dual use research of concern |
| ☒ | ☐ Plants |

## Methods

| n/a | Involved in the study |
|---|---|
| ☒ | ☐ ChIP-seq |
| ☐ | ☒ Flow cytometry |
| ☒ | ☐ MRI-based neuroimaging |

# Antibodies

Antibodies used

Alexa Fluor 594-conjugated anti-mouse CD31 antibody (BioLegend, Cat# 102520, Clone MEC13.3)
FITC-conjugated anti-mouse CD45 antibody (BioLegend, Cat# 157214, Clone S18009F)
BrilliantViolet 421-conjugated anti-mouse EpCAM antibody (BioLegend, Cat# 118225, Clone G8.8)
AlexaFluor 647 conjugated anti-mouse FOXI1 antibody (NovusBio, Cat# NBP2-70747AF647, Clone OTI1D4)
AlexaFluor 594 conjugated anti-mouse Cytokeratin 5 antibody (Santa Cruz, Cat# sc-32721, Clone RCK103)
AlexaFluor 488 conjugated anti-mouse CCSP antibody (Santa Cruz, Cat# sc-390313, Clone B-6)
AlexaFluor 647 conjugated anti-mouse acetylated Tubulin antibody (Santa Cruz, Cat# sc-23950, Clone 6-11B-1)
AlexaFluor 488-conjugated anti-mouse Cytokeratin 5 antibody (Santa Cruz, Cat# sc-32721, Clone RCK103)
AlexaFluor 647-conjugated anti-mouse acetylated Tubulin antibody (Santa Cruz, Cat# sc-23950, Clone 6-11B-1)
AlexaFluor 488-conjugated anti-mouse CCSP antibody (Santa Cruz, Cat# sc-390313, Clone B-6).
AlexaFluor 647-conjugated anti-mouse Cytokeratin 5 antibody (Santa Cruz, Cat# sc-32721, Clone RCK103)
AlexaFluor 647-conjugated anti-mouse acetylated Tubulin antibody (Santa Cruz, Cat# sc-23950, Clone 6-11B-1)
AlexaFluor 647-conjugated anti-mouse CCSP antibody (Santa Cruz, Cat# sc-390313, Clone B-6).
DyLight 550-conjugated anti-tdTomato antibody (Antibodies-online, Cat# ABIN7273113, Polyclonal)
Alexa Fluor 546-conjugated anti-mouse CFTR antibody (Santa Cruz, Cat# sc-376683, Clone A-3)
FITC-conjugated anti-GFP antibody (Santa Cruz, Cat# sc-9996, Clone B-2)
Purified anti-β-actin Antibody (BioLegend, Cat# 643802, Clone 2F1-1)
HRP Goat anti-mouse IgG (minimal x-reactivity) Antibody (BioLegend, Cat# 405306, Clone Poly4053)
Anti-human CFTR monoclonal antibody 596 (CFFT, Clone 596).

Validation

ll antibodies have been validated for target specificity and applications by the manufacturers and published literature:
Alexa Fluor 594-conjugated anti-mouse CD31 antibody (https://www.biolegend.com/en-us/products/alexa-fluor-594-anti-mouse-cd31-antibody-9633)
FITC-conjugated anti-mouse CD45 antibody (https://www.biolegend.com/en-us/products/fitc-anti-mouse-cd45-antibody-21256)
BrilliantViolet 421-conjugated anti-mouse EpCAM antibody (https://www.biolegend.com/en-us/products/brilliant-violet-421-anti-mouse-cd326-ep-cam-antibody-9964)
AlexaFluor 647 conjugated anti-mouse FOXI1 antibody(https://www.novusbio.com/products/foxi1-antibody-oti1d4_nbp2-70747af647)
AlexaFluor 594 conjugated anti-mouse Cytokeratin 5 antibody (https://www.scbt.com/p/cytokeratin-5-antibody-rck103)
AlexaFluor 488 conjugated anti-mouse CCSP antibody (https://www.scbt.com/p/cc10-antibody-b-6)
AlexaFluor 647 conjugated anti-mouse acetylated Tubulin antibody (https://www.scbt.com/p/acetylated-alpha-tubulin-antibody-6-11b-1)
AlexaFluor 488-conjugated anti-mouse Cytokeratin 5 antibody (https://www.scbt.com/p/cytokeratin-5-antibody-rck103)
AlexaFluor 647-conjugated anti-mouse acetylated Tubulin antibody (https://www.scbt.com/p/acetylated-alpha-tubulin-antibody-6-11b-1)
AlexaFluor 488-conjugated anti-mouse CCSP antibody (https://www.scbt.com/p/cc10-antibody-b-6).
AlexaFluor 647-conjugated anti-mouse Cytokeratin 5 antibody (https://www.scbt.com/p/cytokeratin-5-antibody-rck103)
AlexaFluor 647-conjugated anti-mouse acetylated Tubulin antibody (https://www.scbt.com/p/acetylated-alpha-tubulin-antibody-6-11b-1)
AlexaFluor 647-conjugated anti-mouse CCSP antibody (https://www.scbt.com/p/cc10-antibody-b-6).
Alexa Fluor 546-conjugated anti-mouse CFTR antibody (https://www.scbt.com/p/cftr-antibody-a-3)
DyLight 550-conjugated anti-tdTomato antibody (https://www.antibodies-online.com/antibody/7177412/anti-tdTomato+Fluorescent+Protein+tdTomato+antibody+DyLight+550/)
FITC-conjugated anti-GFP antibody (https://www.scbt.com/p/gfp-antibody-b-2)
Purified anti-β-actin Antibody (https://www.biolegend.com/en-us/products/purified-anti-beta-actin-antibody-5714)
HRP Goat anti-mouse IgG (minimal x-reactivity) Antibody (https://www.biolegend.com/en-us/products/hrp-goat-anti-mouse-igg-minimal-x-reactivity-1395)
anti-CFTR monoclonal antibody 596 (https://cftrantibodies.web.unc.edu/available-antibodies/).

# Eukaryotic cell lines

Policy information about cell lines and Sex and Gender in Research

Cell line source(s)

Human lung epithelial BEAS-2B cells, HBE cells, and HBE G542X cells were generously provided by Dr. Hillary Valley and the Cystic Fibrosis Foundation Therapeutics Lab. Primary ferret airway epithelial cells were kindly provided by Dr. Ziying Yan, Dr. Yinghua Tang, and Dr. John F. Engelhardt from the University of Iowa. Primary intestinal stem cells were isolated and cultured following a standard protocol.

| | |
|---|---|
| Authentication | Cell lines were authenticated based on morphology and growth characteristics following the supplier's guidelines during the study. |
| Mycoplasma contamination | All cells were tested, and no mycoplasma contamination was detected. |
| Commonly misidentified lines (See ICLAC register) | No commonly misidentified cell lines were used. |

## Animals and other research organisms

Policy information about studies involving animals; ARRIVE guidelines recommended for reporting animal research, and Sex and Gender in Research

| | |
|---|---|
| Laboratory animals | C57BL/6, B6.Cg-Gt(ROSA)26Sortm9(CAG-tdTomato)Hze/J (Ai9), and C57BL/6J-Gt(ROSA)26Sorem1Crx/J (LumA) mice were purchased from The Jackson Laboratory. B6-Tg(CFTRG542X)Cwr (CFTR G542X) mice were kindly provided by Dr. Craig A. Hodges from the Cystic Fibrosis Mouse Models Core, as well as Dr. Amy Wong and Krista Antonio from the SickKids Research Institute. ROSA\(^{mTmG}\) transgenic ferrets were generously provided by Dr. Ziying Yan, Dr. Yinghua Tang, and Dr. John F. Engelhardt from the University of Iowa. |
| Wild animals | This study did not involve wild animals. |
| Reporting on sex | Both male and female mice were used in this study. |
| Field-collected samples | The study did not involve samples collected from the field. |
| Ethics oversight | All animal studies were approved and conducted in compliance with the University Health Network Animal Resources Centre guidelines (AUP#: 6842 and AUP#: 6856). |

Note that full information on the approval of the study protocol must also be provided in the manuscript.

## Plants

| | |
|---|---|
| Seed stocks | No research involving plants was done in this study. |
| Novel plant genotypes | No research involving plants was done in this study. |
| Authentication | No research involving plants was done in this study. |

## Flow Cytometry

### Plots

Confirm that:

☒ The axis labels state the marker and fluorochrome used (e.g. CD4-FITC).

☒ The axis scales are clearly visible. Include numbers along axes only for bottom left plot of group (a 'group' is an analysis of identical markers).

☒ All plots are contour plots with outliers or pseudocolor plots.

☒ A numerical value for number of cells or percentage (with statistics) is provided.

### Methodology

| | |
|---|---|
| Sample preparation | The tissues were minced into small pieces and transferred to a 50 mL tube containing 5 mL of digestion media (DMEM, 300 U/mL collagenase IV, 100 U/mL DNase I). The tube was incubated at 37°C with shaking (200 rpm) for 30 minutes. After incubation, the lung cell solution was filtered through a 70 µm strainer into a fresh tube, rinsed with 10 mL of wash buffer (ice-cold PBS, 1% FBS), and centrifuged at 1000 rpm for 5 minutes. The supernatant was discarded, and the pellet was resuspended in 10 mL of wash buffer, followed by another centrifugation step.<br><br>The resulting pellet was treated with 5 mL of RBC lysis buffer (Thermo Scientific, Cat# 00-4333-57) for 5 minutes at room temperature to remove red blood cells. The lysis reaction was quenched with 10 mL of wash media, and the sample was centrifuged at 1000 rpm for 5 minutes. The final cell pellet, free of red blood cells, was resuspended in 5 mL of cell staining buffer (ice-cold PBS, 1% BSA) and subsequently stained with antibodies for flow cytometry. |

| | |
|---|---|
| Instrument | CytoFLEX S flow cytometer (Beckman Coulter, Inc, USA). |
| Software | Collection: CytExpert; Analysis: FlowJo v10 |
| Cell population abundance | Cell populations were generally well-separated, and the maximum number of events was collected from the starting sample whenever possible. |
| Gating strategy | Gating was initially based on FSC/SSC to select single cells for further analysis. The cell populations were then analyzed based on marker expression, and subsequent gating was performed based on positive marker levels. |

☒ Tick this box to confirm that a figure exemplifying the gating strategy is provided in the Supplementary Information.